Spectroscopic Studies of the Coupled Binuclear Ferric Active Site in Methemerythrins and Oxyhemerythrin: The Electronic Structure of Each Iron Center and the Iron–Oxo and Iron–Peroxide Bonds

Richard C. Reem,[†] James M. McCormick,[†] David E. Richardson,[†] Frank J. Devlin,[‡] Philip J. Stephens,[‡] Ronald L. Musselman,[§] and Edward I. Solomon*,[†]

Contribution from the Department of Chemistry, Stanford University, Stanford, California 94305, Department of Chemistry, University of Southern California, Los Angeles, California 90089, and Department of Chemistry, Franklin and Marshall College, Lancaster, Pennsylvania 17604. *Received June 10, 1988*

Abstract: The electronic transitions of the binuclear ferric active site of methemerythrin and oxyhemerythrin (oxyHr) are assigned using variable temperature circular dichroism and polarized single crystal absorbance spectroscopies. These transitions are correlated with crystallographic information to obtain insight into the electronic structure of the oxo-bridged binuclear high spin ferric active site. Ligand field bands are assigned to each iron, and the energy shifts of these bands with variation of exogenous ligand are used to evaluate the ligand field strength of these ligands, particularly the peroxide of oxyHr. Peroxide is found to bind as a very strong field ligand, with both strong σ-donor and very weak π-donor character. The exogenous ligand to Fe(III) charge-transfer spectrum shows that both azide and peroxide have a strong bonding interaction at the active site in addition to the bond to the iron. This is consistent with protonation of the peroxide as suggested from earlier Raman data and with the ligand field strength of peroxide in oxyHr. The intense UV transitions are assigned as oxo–Fe charge transfer and are used to generate a model of the electronic structure of the oxo-bridged iron dimers and in particular the change in the Fe–oxo bond with variation in Fe–O–Fe angle. These results provide insight into the reversible binding of dioxygen by the Hr active site.

The binuclear ferric [Fe(III)Fe(III)] oxidation state of hemerythrin (Hr), the oxygen-carrying protein found in the blood of a number of marine invertebrates, has been studied in reasonable detail.[1] It is well-established that these forms, oxyhemerythrin (oxyHr) and the methemerythrin derivatives, have two antiferromagnetically coupled high-spin ferric ions in each monomeric unit of the usually octameric protein.[2] A number of spectroscopic and model compound studies indicate that the large antiferromagnetic exchange coupling is mediated by an oxo bridge.[3] In the native oxyhemerythrin each dimeric iron site binds a single dioxygen molecule as peroxide, which can be replaced by a single anion, yielding the metX^- Hr derivatives.[1] Resonance Raman[4] and single crystal polarized absorbance spectroscopies[5] have shown that dioxygen is bound asymmetrically as peroxide, to a single iron. Other anions (X^- = N_3^-, OCN^-, SCN^-, $SeCN^-$, F^-, Cl^-, Br^-, I^-, NCN^{2-}, NO_2^-, CN^-, and OH^-, thus far) bind to the binuclear ferric unit in a similar manner. Recently it has been advanced that the peroxide bound in oxyHr is protonated and hydrogen bonded to the oxo bridge.[6]

The 2.0 Å resolution crystal structure of the octameric coelomic protein from *T. dyscritum* shows[7] the two irons of the azidomethemerythrin (metN_3^-Hr) active site bridged by two carboxylato side chains as well as the oxo dianion. The Fe–O–Fe angle in this tribridged site is ~130°. One iron (3-his) is bound to three imidazoles from histidine residues, while the other iron (2-his) binds two histidines and the exogenous ligand. The azide anion is linear, forming a bond angle of 111° with the iron and ~30° with the iron–oxo bond. (From an electron density difference map, it is believed that peroxide binds much the same way in oxy.[8]) Another crystal structure[7] shows that the met"H_2O"[9] form of the protein contains a five-coordinate iron (2-his), with no exogenous ligand bound and an open coordination site cis to the oxo bridge.

Now that the geometric structure of the binuclear ferric site is known in some detail, it is important to correlate the spectroscopy with the crystallography, in order to obtain detailed information into the electronic structure of the active site. It is of particular interest to probe the contributions of the oxo bridging unit to the overall stability of the site and the nature of the peroxide–iron bond, which is vitally important to the reversibility of the oxygenation reaction. These questions are best addressed through studies of the d–d and ligand-to-iron charge-transfer transitions of the binuclear iron active site, thus probing the ligand field at the metal and the nature of the ligand–metal bond.

The solution absorbance and circular dichroism (CD) spectra for metCl^-Hr are shown in Figure 1. Chloride is assumed to be a typical "innocent" ligand, in that it does not produce intense, low-energy ligand-to-metal charge-transfer (LMCT) features for Fe(III).[10] Data are displayed from 300 nm, where intense protein side-chain absorbance features dominate, to 1300 nm, which includes the lowest energy electronic absorbance bands seen in ferric Hr. The two intense features at about 330 and 370 nm, the "oxo dimer bands", are present in oxy and all met derivatives.[11]

[†] Stanford University.
[‡] University of Southern California.
[§] Franklin and Marshall College.

(1) (a) Okamura, M. Y.; Klotz, I. M. *Inorganic Biochemistry*; Eichhorn, G. L., Ed.; Elsevier: 1973; pp 320–343. (b) Kurtz, D. M., Jr.; Shriver, D. F.; Klotz, I. M. *Coord. Chem. Rev.* **1977**, *24*, 145–178. (c) Klippenstein, G. L. *Am. Zool.* **1980**, *20*, 39–51.

(2) (a) Moss, T. H.; Moleski, C.; York, J. L. *Biochemistry* **1971**, *10*, 840–842. (b) Dawson, J. W.; Gray, H. B.; Hoenig, H. E.; Rossman, G. R.; Schredder, J. M.; Wang, R.-H. *Biochemistry* **1972**, *11*, 461–465. (c) Okamura, M. Y.; Klotz, I. M.; Johnson, C. E.; Winter, M. R. C.; Williams, R. J. P. *Biochemistry* **1969**, *8*, 1951–1958. (d) Clark, P. E.; Webb, J. *Biochemistry* **1981**, *20*, 4628–4632.

(3) Schugar, H. J.; Rossman, G. R.; Barraclough, C. G.; Gray, H. B. *J. Am. Chem. Soc.* **1972**, *94*, 2683.

(4) (a) Dunn, J. B. R.; Shriver, D. R.; Klotz, I. M. *Proc. Natl. Acad. Sci. U.S.A.* **1973**, *70*, 2582–2584. (b) Kurtz, D. M., Jr.; Shriver, D. R.; Klotz, I. M. *J. Am. Chem. Soc.* **1976**, *98*, 5033–5035.

(5) Gay, R. R.; Solomon, E. I. *J. Am. Chem. Soc.* **1978**, *100*, 1972–1973.

(6) (a) Shiemke, A. K.; Loehr, T. M.; Sanders-Loehr, J. *J. Am. Chem. Soc.* **1986**, *108*, 2437–2443. (b) Shiemke, A. K.; Loehr, T. M.; Sanders-Loehr, J. *J. Am. Chem. Soc.* **1984**, *106*, 4951. (c) Freier, S. M.; Duff, L. L.; Shriver, D. F.; Klotz, I. M. *Arch. Biochem. Biophys.* **1980**, *205*, 449.

(7) Stenkamp, R. E.; Sieker, L. C.; Jensen, L. H. *J. Am. Chem. Soc.* **1984**, *106*, 618–622.

(8) Stenkamp, R. E.; Sieker, L. C.; Jensen, L. H.; McCallum, J. D.; Sanders-Loehr, J. *Proc. Natl. Acad. Sci. U.S.A.* **1985**, *82*, 713–716.

(9) The terminology for met"H_2O" or met"aquo" Hr is from early work on the protein[11] which indicated H_2O was bound to the metal site.

(10) Note, however, a weak $Cl^- \rightarrow$ Fe(III) CT transition does, in fact, contribute to the 300–400-nm region (vide infra).

(11) Garbett, K.; Darnall, D. W.; Klotz, I. M.; Williams, R. J. P. *Arch. Biochem. Biophys.* **1969**, *135*, 419–434.

0002-7863/89/1511-4688$01.50/0

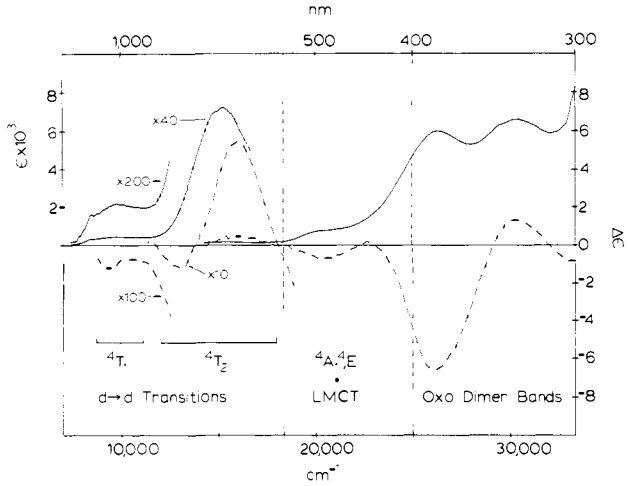

Figure 1. Room temperature solution CD (- -) and absorbance (—) spectra for metCl⁻Hr. The three regions from right to left are dominantly iron-oxo dimer bands, Fe(III) ligand field or exogenous LMCT, and Fe(III) ligand field transitions, respectively.

These transitions are also observed in a number of iron–oxo dimer model complexes[6,11,12] and have been variously assigned as oxo–iron charge transfer (CT)[13] or simultaneous pair excitation (SPE) transitions.[3] The second region, lying between 400 and 550 nm, contains ligand field transitions from the ferric irons and exogenous ligand-to-iron CT bands for certain "noninnocent" ligands (N_3^-, SCN^-, O_2^{2-}). Since the ligand field bands are relatively weak, this region allows a direct study of the electronic structure of these exogenous ligands, particularly azide and peroxide. The final region, from 550 to ~1200 nm, contains only Fe(III) ligand field transitions. This study examines these three spectral regions in some detail.

The ligand field bands in the near IR spectral region are used to describe the electronic structure of each iron and the effect of changing exogenous ligands. High-spin ferric iron has five unpaired d electrons, producing a $^6A_1$ ground state. As this is the only sextet spin state, all d–d transitions in high-spin Fe(III) are spin and Laportê forbidden, generally resulting in very weak transitions ($\epsilon < 1$ cm^{-1} M^{-1}).[14] The observed transitions terminate at quartet spin excited states. The lowest energy of these states is the $^4T_1$ state, with the $^4T_2$ and $^4A_1$,^4E levels to increasingly higher energy. The transitions to the $^4T_1$ and $^4T_2$ states, generally occurring in the 600 to 1200 nm spectral region, are very sensitive to the strength of the ligand field at the iron and thus give information on the effects of ligands binding to the iron center. The $^4A_1$,^4E transition is ligand field independent, consisting of only a spin flip in the e_g orbitals and thus gives a sharp absorbance band near 400–500 nm. This transition gives information on the electron–electron repulsion at the iron and thus on covalency.[15] Gray and co-workers[16] assigned a band at ~480 nm in metHr as the $^4A_1$,^4E transition and broader bands near 650 and 1000 nm as $^4T_2$ and $^4T_1$ transitions, respectively.

Charge-transfer transitions involve promotion of an electron from a filled ligand valence orbital to one of the half-filled Fe(III) d orbitals. The excited state can be pictured as a d^6 Fe(II) ion, plus the ligand shell with a hole in the valence orbital. Electron–electron repulsion on the metal must be considered, but interaction with the hole on the ligand is small, allowing compilation of the symmetries of all excited states that arise from each one-electron promotion. While there are several excited states for each such transition, only one is spin- and symmetry-allowed in each case. This is because the spin sextet ground state of high-spin Fe(III) makes accessible only those CT excited states involving quintet states of the resultant Fe(II). The problem thus reduces to a simple one-electron picture, with results directly relating to bonding of the ligand involved in the CT transition.

The dimer bands in the 300–400-nm region are analyzed to yield information on the iron–oxo bridge, particularly relating to the angle and strength of the oxo–iron bond, and thus its possible involvement in the reversible binding of dioxygen. Study of the exogenous ligand charge-transfer transitions provides detailed insight into the exogenous ligand–iron bond. Of particular interest is the peroxide–iron bond and its relation to the reactivity of this protein active site.

Experimental Section

Protein was isolated as oxyhemerythrin from the coelomic fluid of *Phascolopsis gouldii*, which were obtained live from Marine Biological Laboratories, Woods Hole, MA. The protein was purified by the standard methods[17] and then dialyzed into 0.1 M Tris SO_4 (pH 7.7) buffer for storage and most experiments. For prolonged storage, the oxygenated protein was frozen in LN_2. Protein concentration is expressed in terms of protein monomers and was determined spectroscopically by measuring the 500-nm absorbance band in oxyHr, the 446-nm band in $MetN_3^-$, or the intense UV features of the nonchromophoric ligands.[11] Met"H_2O" Hr was prepared by dialyzing oxyHr overnight against ~5 mM $Fe(CN)_6^{3-}$ and subsequently dialyzing several times against the Tris buffer. The metX⁻ Hr derivatives were then obtained by dialyzing the met"H_2O" sample against the desired concentration of anion. This varied from 0.01 M NaN_3 to ~0.1 M for most anions, to as much as 1 M KI for the weak binding iodide complex.[18]

Single crystals of the protein for polarized absorbance measurements were grown by placing an appropriate concentration (usually about 2 mM) of the desired derivative into a glass tube with dialysis tubing closing off each end. The tube was placed into an evaporation dish containing the appropriate buffer (including ligand) and 10–20% ethanol. This dish was placed into a closed container, which contained a similar solution (with 25% EtOH) to keep the ethanol concentration in the dish constant. The tube was monitored until crystals of necessary size (~0.3 × 0.3 × 5 mm) were present (2–5 days). The crystals were stored in the mother liquor at 4 °C. Crystals of the necessary thickness to obtain data in the desired spectral range were drawn into a Pasteur pipet and placed onto a quartz disc. Only enough mother liquor was removed to cause the crystal to stick to the disc and to avoid depolarization of incident light. A lightly greased O-ring spacer and another disc were then placed on top. Both discs were then masked with black tape such that light must pass through the crystal. The spectra were obtained with a McPherson RS-10 spectrophotometer with a 2510 one-meter monochrometer, equipped with specially designed sample chamber with focussing optics and Glan-Taylor polarizers.

The needle-shaped hemerythrin crystals were of the *P*422 tetragonal space group, with two octamers, and therefore 16 iron dimers per unit cell.[19] Polarized single-crystal spectra were obtained with the **e** vector of light oriented $\parallel$ and $\perp$ to the *c* axis.[20] The Fe-Fe vector of each site is aligned along the *c* axis, thus any transition polarized along this vector will appear strongly parallel polarized. As the Fe–O–Fe angle is ~130°, the Fe–O vector is tilted ~25° off the *c* axis. Thus a transition polarized along this bond would appear mostly in the $\parallel c$ spectrum but would also make a small contribution of $\sin^2 25° = 0.18$ to the $\perp c$ polarized spec-

(12) (a) Armstrong, W. H.; Spool, A.; Papaefthymiou, G. C.; Frankel, R. B.; Lippard, S. J. *J. Am. Chem. Soc.* **1984**, *106*, 3653. (b) Wieghardt, K.; Pohl, K.; Gebert, W. *Angew. Chem.* **1983**, *95*, 739. (c) Spool, A.; Williams, I. D.; Lippard, S. J. *Inorg. Chem.* **1985**, *24*, 2156.

(13) (a) Solomon, E. I.; Wilcox, D. E. Magneto-Structural Correlations in Bioinorganic Chemistry. In *Magneto-Structural Correlations in Exchange Coupled Systems*; NATO-ASI: June 1983; Reidel: 1985; p 463. (b) McCallum, J. D.; Shiemke, A. K.; Sanders-Loehr, J. *J. Biochemistry* **1984**, *24*, 2819.

(14) Holt, S.; Dingle, R. *Acta Chem. Scand.* **1968**, *22*, 1091.

(15) Fergusen, J. Spectroscopy of 3d Complexes. In *Progress in Inorganic Chemistry*; Lippard, S. J., Ed.; Wiley-Interscience: 1979; Vol. 12, pp 159–294.

(16) Loehr, J. S.; Loehr, T. M.; Mauk, A. G.; Gray, H. B. *J. Am. Chem. Soc.* **1986**, *102*, 6992–6996.

(17) Klotz, I. M.; Klotz, T. A.; Fiess, J. A. *Arch. Biochem. Biophys.* **1957**, *68*, 284–299.

(18) Incomplete conversion and distinct isomeric complexes can be ruled out for two reasons. First, conversions can be followed with time and concentration, and any unconverted sample would be easily recognized by either CD or absorbance. Second, Raman spectra always show only one M–oxo or M–L vibration, and since this technique should be more sensitive to multiple conformations than electronic spectroscopy, only one species is present for each metX⁻ derivative (except for metI⁻, which is not completely converted).

(19) (a) Stenkamp, R. E.; Sieker, L. C.; Jensen, L. H. *Proc. Natl. Acad. Sci. U.S.A.* **1976**, *73*, 349. (b) Ward, K. B.; Hendrickson, W. A.; Klippenstein, G. L. *Nature* **1975**, *257*, 818.

(20) Verification of proper crystal morphology and axis alignment were made using a polarizing microscope. Crystal shape and extinction were identical with that described previously.[19b]

Table I. $^4T_1$ Transitions of MetX$^-$ Hemerythrin in CD and Absorbance

ligand	CD ν_{max} (cm^{-1})	$\Delta\epsilon$ (M^{-1} cm^{-1})	abs ν_{max} (cm^{-1})	ϵ (M^{-1} cm^{-1})
OCN^-	9090	-0.0113	9800	10.2
N_3^-	9800	-0.031	9850	13.0
SCN^-	9170	-0.0123	9800	11.2
CN^-	*a*	*a*	~9800	~14
Cl^-	9260	-0.0119	9800	11.0
OH^-	9700	+0.0090	10100	10.6
"H_2O"	11000	-0.016	~10600	~7.0

[a] A negative signal is observed, but the maximum could not be determined.

trum. The final structural feature of interest in the polarized studies is the orientation of the exogenous ligand-Fe bond which is $\perp$ to the Fe–Fe vector, and thus an exogenous ligand to Fe(III) CT transition (which is polarized along this bond) should appear strongly polarized in the $\perp c$ orientation.

Solution absorbance spectra employed a Cary-17 spectrometer. CD studies were performed on a JASCO J-500C spectropolarimeter in the 300–1100 nm wavelength range, and extension to 2000 nm was obtained on a home-built instrument.[21] For low-temperature studies, glassing samples were prepared by dialysis against saturated sucrose/buffer solutions.[22] Glycerol (60%) + high anion concentration was also used to produce glassing, giving identical spectra but slightly inferior glasses and therefore worse signal/noise. The prepared sample was placed between quartz discs with a rubber O-ring spacer of desired thickness (0.5–3 mm) and cooled using an Air Products cryotip. For the low-temperature CD studies, a nickel tartrate sample was placed alternately before and after the sample, and, if identical CD spectra resulted, this showed the frozen sample was not being strained and was not depolarizing the incident light. Regions of the spectrum with no CD signal were shown to be coincident at varying temperatures, indicating that the base line had not shifted.

The near-IR absorbance and CD data were obtained on samples with the solvent H_2O replaced with D_2O. This was obtained by repeated concentration to 1 mL with an Amicon ultrafiltration cell and subsequent 10× dilution with 0.1 M $TrisSO_4$ pD 8.1 buffer in D_2O, with the appropriate ligand.

Resonance Raman studies required samples having absorbance 2-3 for a 1-cm path at the wavelength of the exciting laser light. Na_2SO_4 at concentrations of 0.1-1.0 M was used as an internal standard. Samples were run in a spinning cell with scattered light collected at 90°. The instrument has been described previously.[23]

Single-crystal spectra of $enH_2[(FeHEDTA)_2O]\cdot 6H_2O$ were taken on the McPherson spectrometer on various crystal faces[3] to obtain three orientations of the electric field vector with respect to the Fe–O–Fe plane and Fe–Fe vector. Polarized specular reflectance studies were performed on natural crystal faces using a specially constructed instrument.[24] Polarized absorbance data were derived from the Kramers–Kronig transformation of the absolute reflectivity data. The technique is based upon the Fresnel relationship between absorptivity coefficient, reflectivity, and phase change upon reflection.[24]

Results

Ligand Field Transitions. Three sets of ligand field transitions are observed over the spectral range of 400–1300 nm for each of the metX$^-$Hr derivatives. These bands are labeled as the $^4A_1$,^4E; $^4T_2$, and $^4T_1$ regions in Figure 1. They are identified and assigned based on the changes exhibited with a number of physical and chemical perturbations, combined with ligand field theory for the high-spin ferric ion. These transitions are interpreted below, in order of increasing energy.

$^4T_1$ Region. The $^4T_1$ region of the absorbance spectrum begins near 850 nm and extends further into the near IR, as shown in Figure 1. This region is very difficult to study due to the intense

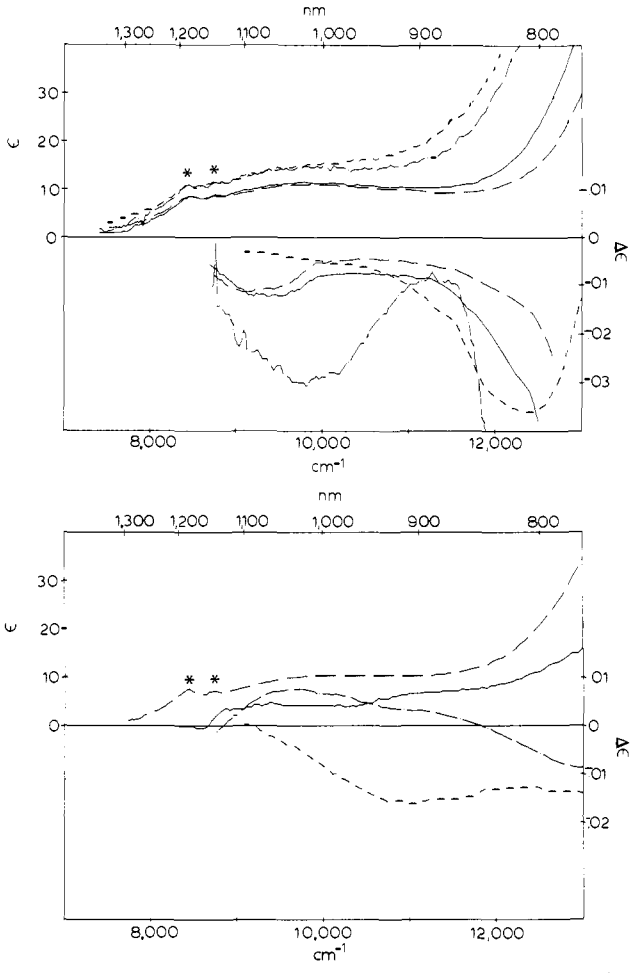

Figure 2. (A) Absorbance (top) and CD (bottom) in the near IR $^4T_1$ region for metCl$^-$Hr (—), metCN$^-$Hr (- -) (shown ×4 in CD), metOCN$^-$HR (— —), and metN_3^-Hr (— · —). (B) MetOH$^-$Hr CD (— · —), absorbance (— —), met"H_2O"Hr CD (- -), and absorbance (—) in the near IR $^4T_1$ spectral region. Features marked with * are from protein vibrational overtones.

vibrational overtones of water. However, in D_2O the absorbance spectrum is accessible out to nearly 2000 nm. The very low intensity of the $^4T_1$ transitions requires highly concentrated samples in order to observe the signals,[16] which are seen as weak, broad, and poorly resolved bands. Spectra of much higher quality can be obtained in this region using near-IR CD. The absorption and CD spectra for a number of met complexes are given in Figure 2 and summarized in Table I.

Figure 2 shows the $^4T_1$ transitions in metHr derivatives present at approximately the energy expected for octahedral Fe(III).[14,15] These bands shift when the site is perturbed by exchanging exogenous ligands. The molar extinction coefficients of these signals, although weak (~10 cm^{-1} M^{-1}), are much more intense than expected for Fe(III) monomers; iron-oxo dimer model complexes do show bands of similar energy and intensity.[3,12] While the weak, broad nature of these bands precludes detailed interpretation, the observation that the $^4T_1$ bands in met"H_2O" Hr (Figure 2b) are at significantly higher energy than those of all other metX$^-$ derivatives is important.

$^4T_2$ Region. The next higher energy group of electronic absorbance bands in Figure 1 is associated with the $^6A_1 \rightarrow {}^4T_2$ transition, which is observed in the region between 550 and 850 nm. These bands are much more intense ($\epsilon \approx 160$ cm^{-1} M^{-1}) than the $^4T_1$ transitions, allowing for detailed interpretation. Figure 3 shows the temperature dependence of the $^4T_2$ region in metOCN$^-$Hr. The room temperature absorbance spectrum shows a single peak at 650 nm (15 400 cm^{-1}), which gains intensity and moves to lower energy as the temperature is decreased. The high-energy side of the band is very broad (especially apparent

(21) (a) Osborne, G. A.; Cheng, J. C.; Stephens, P. J. *Rev. Sci. Instrum.* **1973**, *22*, 2160. (b) Nafie, L. A.; Keiderling, T. A.; Stephens, P. J. *J. Am. Chem. Soc.* **1976**, *98*, 2715.

(22) This dialysis resulted in substantial concentrating of the sample, and therefore a known volume of the saturated sucrose solution was added directly to the original protein solution to control the final concentration.

(23) Pate, J. E.; Thamann, T. J.; Solomon, E. I. *Spectrochim. Acta, Part A* **1986**, *42*, 313.

(24) (a) Desjardins, S. R.; Penfield, K. W.; Cohen, S. L.; Musselman, R. L.; Solomon, E. I. *J. Am. Chem. Soc.* **1983**, *105*, 4590. (b) Kronig, R. deL. *J. Opt. Soc. Am.* **1926**, *12*, 547.

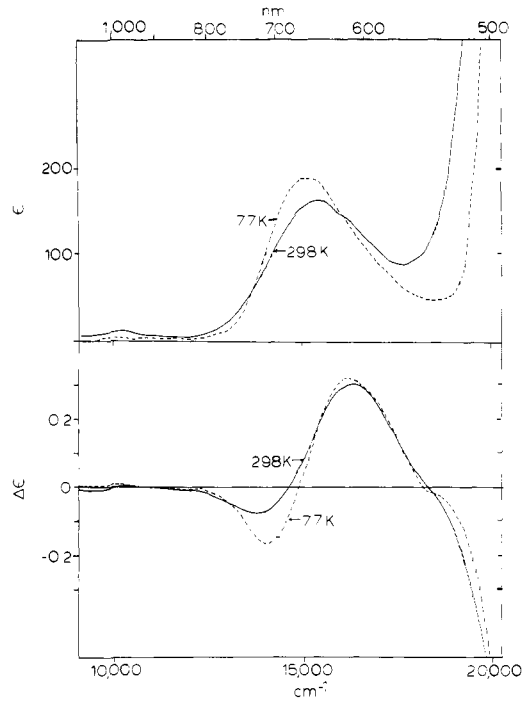

Figure 3. Solution and glass absorbance (top) and CD (bottom) spectra of the $^4T_2$ Fe(III) ligand field transitions in metOCN$^-$Hr at 298 K (—) and 77 K (- -).

at low temperatures), indicating additional transitions in this region. The room temperature CD spectrum shows a positive feature at 620 nm (16 100 cm^{-1}) and a weaker negative feature at 734 nm (13 600 cm^{-1}), neither of which corresponds to the absorbance band maximum. As the sample is cooled, the CD bands do not shift in energy, but the lower energy (negative) component shows a much greater increase in intensity. All metX$^-$Hr derivatives (X$^-$ = Cl$^-$, N_3^-, Br$^-$, CN$^-$, SCN$^-$, SeCN$^-$) show similar temperature dependence in this region.

The energies of these bands are perturbed with variation of the exogenous ligand, as shown in Figure 4. The absorbance data initially appear much as expected, with the bands moving to lower energy upon binding of stronger field ligands. However the high-energy, broadened portion of the spectrum (at 77 K) does not change significantly. The CD spectra are particularly informative, as only the negative, low-energy component shifts significantly when ligands are changed. As seen in Figure 4, metCN$^-$ exhibits this band at lowest energy, as expected for this very strong field exogenous ligand. It is important to note however that oxyHr (Figure 4b) also has a similar low-energy transition.

While the negative CD peak in oxyHr (Figure 4b) is quite intense, the positive feature is extremely weak. Similar behavior is observed in the I$^-$ (Figure 4b) and N_3^- (Figure 5a) derivatives. The temperature dependence of the positive CD peak of these derivatives is also unusual in that several bands become clearly resolved at low temperature, allowing for a gaussian fit of five component transitions in the $^4T_2$ region (see Analysis Section). Figure 5 presents this fit for the CD and absorbance of metN_3^-Hr as well as a similar fit for the "normal" metBr$^-$ data.

Met"H_2O"Hr also exhibits distinctive characteristics, as displayed in comparison to metOH$^-$ in Figure S1 in the Supplementary Material. For met"H_2O"Hr both CD features and the absorbance band occur at much higher energies, indicating a much weaker ligand field. In addition both CD peaks have very low intensities, expecially the positive signal, and the temperature dependence of the absorbance shoulder is clearly different, with no shift and little intensity change as the temperature is decreased. The absorbance and CD $^4T_2$ peak energies and intensities for all metX$^-$Hr derivatives are listed in Table II.

The CD spectra of halfmetX$^-$ ([Fe^{III}Fe^{II}]X$^-$, where X$^-$ = OCN$^-$, CN$^-$, Cl$^-$, N_3^-, and SCN$^-$) are shown in Figure 6 for comparison to the analogus metX$^-$ derivatives. Upon reduction of one iron

Table II. $^4T_2$ Transitions of MetX$^-$ Hemerythrin in CD and Absorbance

ligand	CD ν_{max} (cm^{-1})	$\Delta\epsilon$ (M^{-1} cm^{-1})	abs ν_{max} (cm^{-1})	ϵ (M^{-1} cm^{-1})
Cl$^-$	16 000	+0.485	15 240	180
	13 100	-0.058		
NCS$^-$	16 200	+0.473	14 840	200
	13 700	-0.169		
OCN$^-$	16 260	+0.300	15 390	166
	13 700	-0.073		
Br$^-$	15 500	+0.58	14 770	165
	12 780	-0.121		
CN$^-$	15 390	+0.66	14 390	140
	12 420	-0.137		
I$^-$	14 600	+0.107[a]	13 400[a]	?
	12 330	-0.120[a]		
N_3^-	~15 900	+0.031	14 700	190
	13 250	-0.205		
HO_2^-	~14 000		13 300	200
	12 500	-0.36		
SeCN$^-$	16 000	+0.222	14 700	210
	13 500	-0.285		
OH$^-$	15 850	+0.18	16 750	160
	13 500	-0.013		
"H_2O"	16 390	+0.007	17 240	200
	15 150	-0.035		

[a] Values are only approximate due to a large met"H_2O" impurity contribution.

to give this mixed-valence form, the positive CD feature of the met derivatives near 630 nm is eliminated, leaving the low-energy negative feature in approximately the same position as in the met spectra, with similar intensity. These bands also show an energy shift (although smaller) with variation in ligand. Note that the fairly intense positive CD feature at about 1000 nm corresponds to d–d transitions on the high-spin Fe(II) of the halfmet site.

Finally, Figure S2 in the Supplementary Material gives the single-crystal polarized absorbance data for metCl$^-$Hr, in the $^4T_2$ region. These spectra show that the parallel polarized component is more intense and at lower energy than the feature in perpendicular polarization. Both polarizations gain intensity and move to lower energy as the temperature is lowered.

$^4A_1$, ^4E Region. Figure 7 shows transitions in the region between 400 and 550 nm (18 000–25 000 cm^{-1}) for three met derivatives with innocent exogenous ligands. On the basis of polarized single crystal spectra (vide infra), these metX$^-$ (X$^-$ = Cl$^-$, OCN$^-$, CN$^-$) spectra contain no exogenous ligand → metal CT transitions at wavelengths longer than 400 nm (<25 000 cm^{-1}). With the exception of metI$^-$Hr, the complete series of met derivatives uniformly exhibits a transition near 480 nm in both absorbance and CD which shows very little energy shift upon changing the exogenous ligand.[11] (In metI$^-$Hr this peak is at significantly lower energy, about 515 nm (19 400 cm^{-1}) but is similar to the other derivatives in sign and intensity.) This band can be assigned as the $^4A_1$,^4E transition. In absorbance, the $^4A_1$,^4E band has an extinction coefficient of about 500 cm^{-1} [M^{-1}, while the CD spectrum shows a negative band at this energy with $\Delta\epsilon \approx -0.5$ cm^{-1} M^{-1}. There is, however, a large temperature dependence, with both CD and absorbance showing an intensity increase and small shift to higher energy as the temperature is lowered. The single-crystal absorbance data in Figure 8 show the 480-nm absorbance band to be dominantly parallel to *c* polarized. The resonance Raman excitation profile of the Fe–oxo symmetric stretching vibration at 509 cm^{-1} for metCl$^-$ (also shown in Figure 8) shows no enhancement at 480 nm, indicating that this is likely a d–d transition. This is supported by the halfmet CD spectrum in Figure S3 in the Supplementary Material, where the 480-nm band is still present, but with about half the intensity.

While the resonance Raman profile at the 480-nm band shows no enhancement of the Fe–O stretch, there are two peaks observed in the profile in this 550–400-nm region, one at ~540 nm (seen for metN_3^-, and in Figure 8 for metCl$^-$) and a second at ~430 nm (for metN_3^-).[6b] This indicates that there are weak oxo → Fe(III) CT transitions in this region. The absorbance and CD

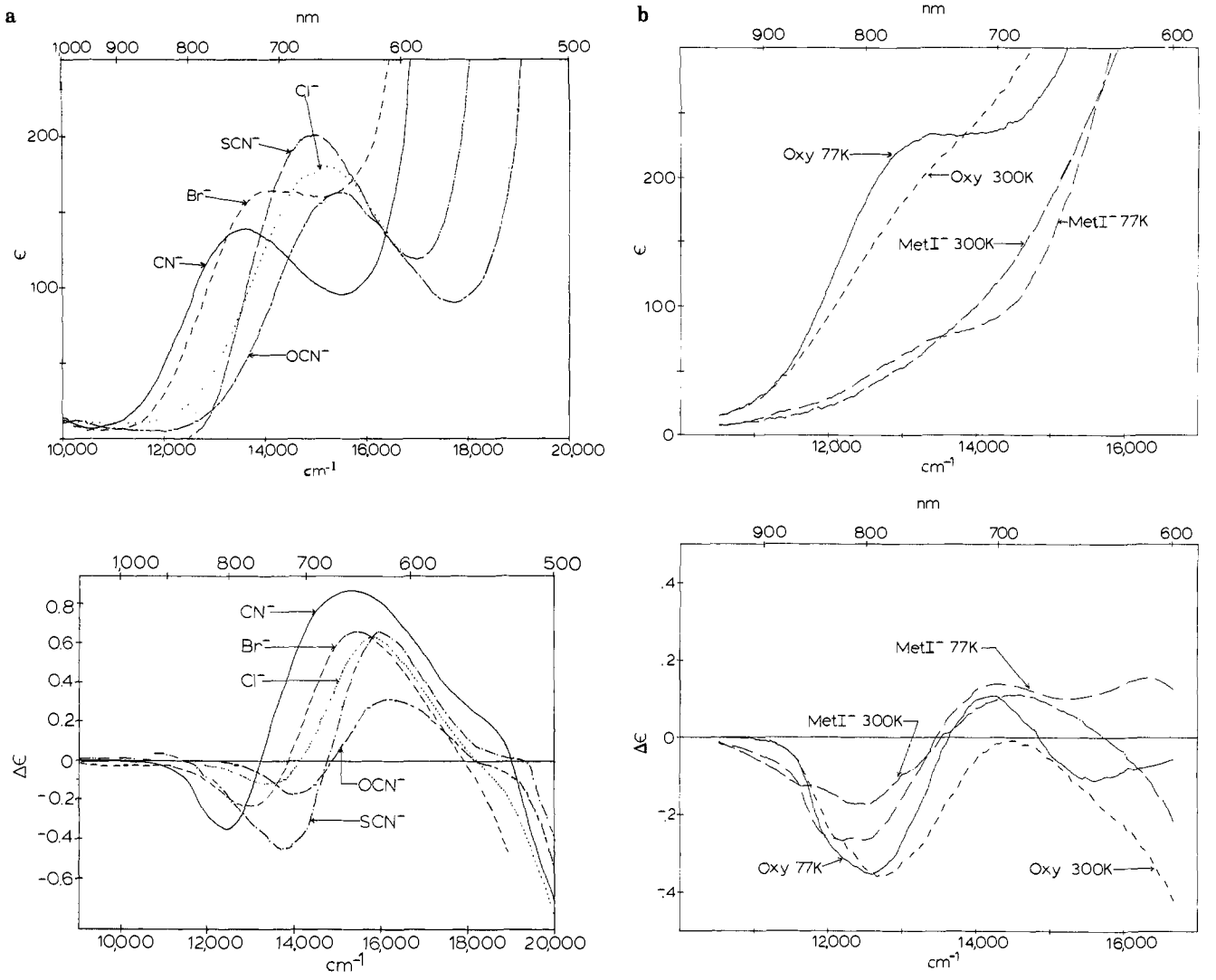

Figure 4. Variation of energy of $^4T_2$ transitions in metX⁻Hr CD with variation of exogenous ligand. (A) Room temperature absorbance (top) and CD (bottom) data for MetX⁻Hr where X⁻ = Cl⁻ (···), OCN⁻ (— — —), CN⁻ (—), SCN⁻ (— · —), and Br⁻ (– –). (B) Absorbance (top) and CD (bottom) for oxyHr at 77 K (—) and 300 K (– –) and metI⁻Hr at 77 K (— —) and 300 K (— · —).

spectra of the metX⁻ compounds with innocent ligands also indicate the presence of additional transitions in this region. As seen, for example, for metCN⁻ in Figure 7c, a transition is visible as a positive CD feature near 430 nm. This 430-nm band is not due to the $^4A_1$,^4E transition originating on one iron, since the 430-nm band is present in some halfmet species (see Figure S3 in the Supplementary Material). In halfmet only one type of Fe(III) is present, and its $^4A_1$,^4E transition is clearly present near 500 nm. At low temperatures, metCl⁻ shows an additional negative CD band at 540 nm, shown in Figure 7b.

Iron–Oxo Dimer Region. The polarized single crystal absorption spectrum of metF⁻Hr given in Figure 8 shows two intense $\|c$ polarized bands in the 300–400-nm region at 27 400 and 30 770 cm⁻¹. These bands also appear weakly in the $\perp c$ spectrum ($I_\perp/I_\| = 0.23$ at 365 nm). These bands are the iron–oxo dimer bands, and based on their polarization ratio they appear to be polarized approximately along the Fe–O bond which is tilted ~25° off the c axis. Fluoride having the highest optical electronegativity of any exogenous ligand studied will exhibit the highest energy exogenous ligand to Fe(III) CT (predicted to be at ~50 000 cm⁻¹). On the basis of the lack of any significant additional $\perp c$ polarized absorption intensity the F⁻ → Fe(III) CT transition must be at higher energy than 33 000 cm⁻¹.

Figure 7 includes the solution absorbance, and CD data in the 300–400 nm region for three metHr derivatives (OCN⁻, Cl⁻, CN⁻) which are also expected to have relatively high-energy exogenous ligand-to-metal CT transitions. These CT transitions could, however, contribute in the 300–400-nm region, and this must be sorted out in order to define the spectral features of the Fe–oxo bands in these derivatives. The metOCN⁻ absorbance spectrum (Figure 7a) exhibits two very intense bands near 330 nm (30 300 cm⁻¹) and 379 nm (26 400 cm⁻¹). As the temperature is lowered, the 379-nm band sharpens slightly but does not shift or change intensity, while the 330-nm band becomes somewhat more intense at low temperature. The CD show a large negative band at 380 nm (26 300 cm⁻¹) and a weak positive band at 334 nm (29 900 cm⁻¹). At LN_2 temperature the 380-nm band shows a broadening and asymmetry to high energy. The CD data can be fit with negative bands at 380 and 353 nm (28 300 cm⁻¹). The metCl⁻ data shown in Figure 7b are very similar to the metOCN⁻ results, with intense absorbance and CD bands at very nearly the same energy and with the same temperature dependence. Again, the negative 380-nm band broadens to high energy and can be fit with bands at 382 and 356 nm (26 200 and 28 100 cm⁻¹). The metCN⁻ data in Figure 7c are again very similar to the Cl⁻ and OCN⁻ derivatives, with one significant difference. The large, negative CD band at 380 nm broadens to low energy at low temperature, being fit to bands at 380 and 398 nm (25 100 cm⁻¹). The bands at 353 nm in the OCN⁻, 398 nm in the CN⁻, and 356 nm in the Cl⁻ derivatives are the only features in this region which move significantly with change of exogenous ligand. These bands must, therefore, arise from exogenous ligand to metal CT and are of approximately the energies expected for these ligands.[25]

(25) (a) Gamlen, G. A.; Jordan, D. O. *J. Chem. Soc.* **1953**, 1453. (b) Day, P. *Inorg. Chem.* **1966**, *5*, 1619.

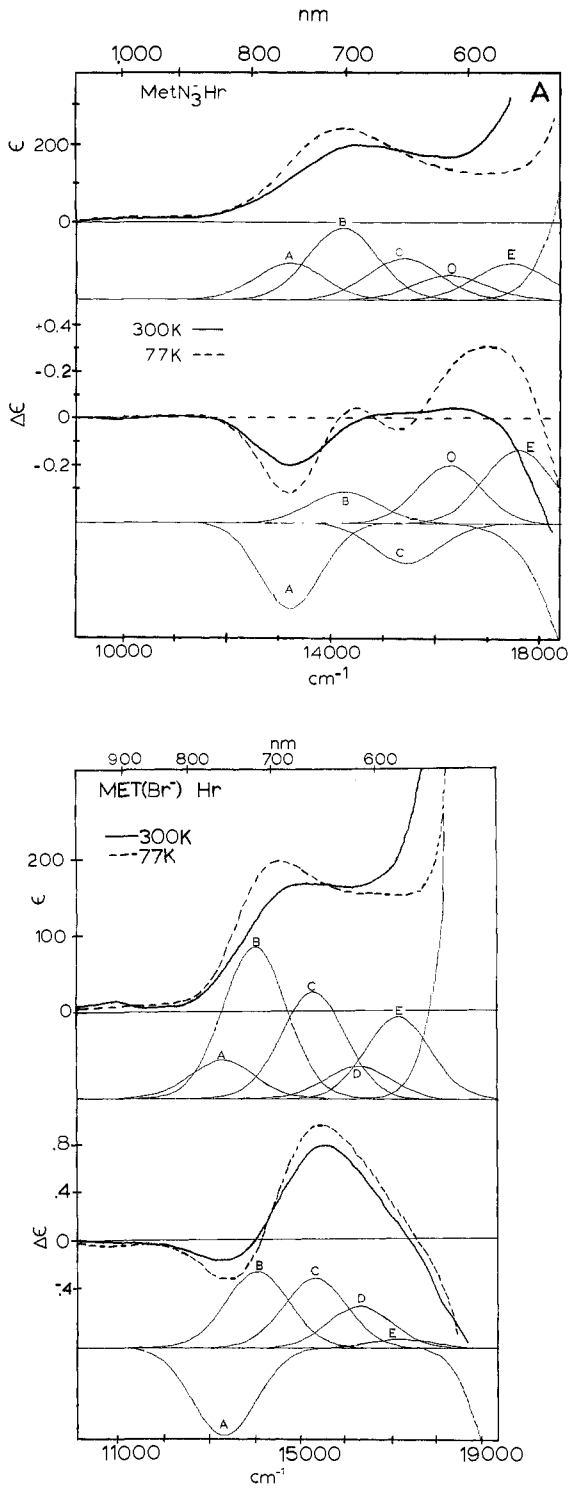

Figure 5. Room temperature (—) and LN_2 (--) absorbance (top) and CD (bottom) spectra for the $^4T_2$ region in $MetN_3^-Hr$ (a) and $metBr^-Hr$ (b). Also shown are gaussian fits (of 77 K data) with the smallest acceptable number of bands for each derivative. See Table V and text for details.

The presence of a $Cl^- \rightarrow$ Fe(III) CT transition in the 300–400-nm region of the $metCl^-$ spectrum can most directly be observed from comparison of its polarized single crystal spectrum with that of $metF^-$ in Figure 8. The $I_\perp/I_\parallel$ ratio of $metCl^-$ at 376 nm is 0.41, which is approximately twice that of $metF^-$ indicating additional $\perp$ polarized intensity in this region which must reflect exogenous ligand to Fe(III) CT. For $metCl^-$ the intensity of the two peaks in the $\perp c$ spectrum is inverted relative to the $\parallel c$ spectrum with the higher energy band being more intense indicating that the $Cl^- \rightarrow$ Fe(III) CT is contributing in the 29000-cm^{-1}

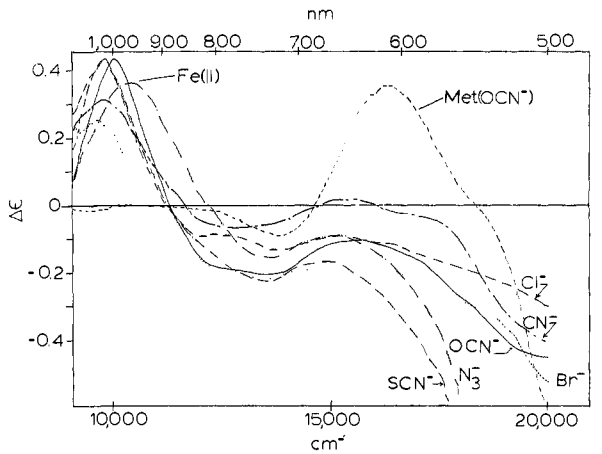

Figure 6. Variation in the $^4T_2$ region of halfmetX^-Hr with change in exogenous ligand. $X^- = SCN^-$ (—·—), N_3^- (—··—), OCN^- (—), Br^- (···), CN^- (— — —), and Cl^- (——). $MetOCN^-Hr$ (--) is shown for comparison.

Table III. Iron–Oxo Dimer Bands

Met	E^a (cm^{-1})	ϵ^a (M^{-1} cm^{-1})
OCN^-	30200	4860
	26400	6100
Cl^-	30450	5660
	26050	6400
N_3^-	30900	4760
	26000	3500
HO_2^- (Oxy)	30800	5500
	27000	4000
models		
A[d]	~36400?[c]	(sh)
	~29850[b]	~3680[b]
	~26800[b]	(sh)
B[e]	35200	4500
	31600	6000
	28100	9000

[a] Intensities and energies from gaussian fit to spectrum. [b] Intensities and energies estimated from absorbance spectrum. [c] Probably not oxo–Fe(III) CT (see text). [d] A = $[Fe_2O(O_2CCH_3)_2(TACN)_2]I_2$ in CH_3CN from ref 11c. [e] B = $[(FeHEDTA)_2O]\cdot 6H_2O$ polarized reflectance.

region consistent with the fit to the CD results given above. It should be noted that all polarized single-crystal spectra of the $metX^-$ derivatives exhibit two similar intense Fe–oxo dimer bands in the $\parallel c$ polarization in the 300–400-nm region (vide infra, $metN_3^-$ and oxyHr). The energies and intensities of these iron–oxo dimer bands for a number of met derivatives are summarized in Table III.

Finally, Figure 8 also includes the resonance Raman excitation profile of the 509 cm^{-1} iron–oxo stretch for $metCl^-$. This vibration is enhanced into the UV although the peak energy could not be determined due to rapid denaturation of the $metCl^-Hr$ at room temperature with UV excitation.[26]

It is important to correlate these results with the UV absorbance data of iron–oxo dimer model complexes. The models of Wieghardt et al.[12b] and Lippard et al.[12a] each contain two irons bridged by two carboxylates and the oxo dianion, with angles very similar to hemerythrin ($\angle$Fe–O–Fe ~130°). Thus far only solution studies have been done, and these show (Figure 9b for the Lippard et al. model) two intense bands near 370 and 330 nm and a weaker band

(26) (a) ν(Fe–O–Fe) enhancement profiles have been reported[6b,26b,c] in the dimer band region which do not simply reflect the absorption intensity. In particular, little enhancement is observed for any vibration from the 330-nm absorption band. (b) Czernuszewicz, R. S.; Sheats, J. E.; Spiro, T. G. *Inorg. Chem.* **1987**, *26*, 2063. (c) Sanders-Loehr, J. Resonance Raman Spectroscopy of Iron-Oxo and Iron-Sulfur Clusters in Proteins. In *Metal Clusters in Proteins*; Que, L. Jr., Ed.; ACS Symposium Series 372; American Chemical Society: Washington, DC, 1987; pp 49–67.

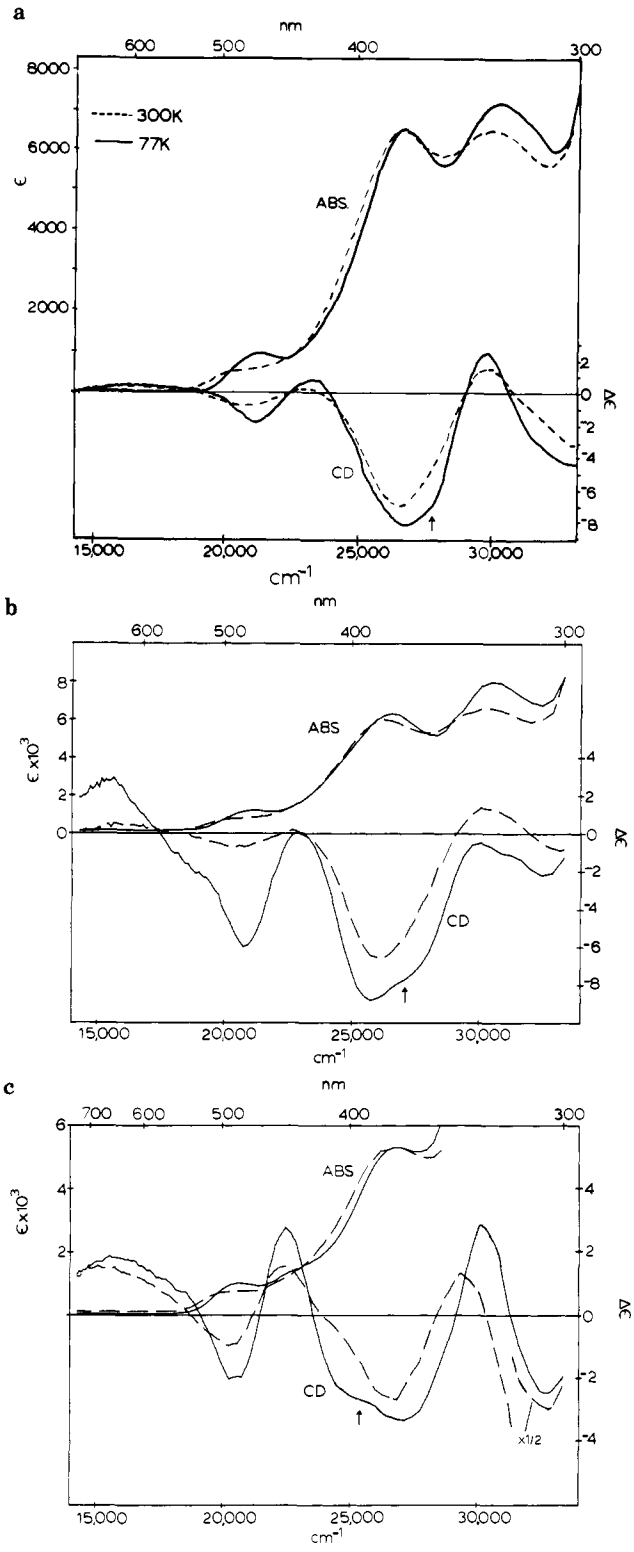

Figure 7. Room temperature (- -) and 77 (—) absorbance (top) and CD (bottom) spectra for metOCN⁻ (a), metCl⁻ (b), and metCN⁻Hr (c). Data cover the two regions on the right side of Figure 1. Arrows indicate positions of exogenous ligand-to-metal charge-transfer transitions.

at 260–270 nm. This region is almost identical with the met Hr $\|c$ spectra in Figure 8, indicating the tribridged metHr species have only two approximately parallel polarized transitions at 370 and 330 nm, and no additional bands are obscured by the 280-nm protein absorbance. In addition there are a number of weaker bands between 400 and 550 nm. The Raman enhancement profile reported[12c,26b,c] is similar to that of metCl⁻ and metN$_3$⁻Hr,[6b,c,26c] with one weak feature at about 520 nm and another variably at 440–480 nm, with more enhancement in the UV.

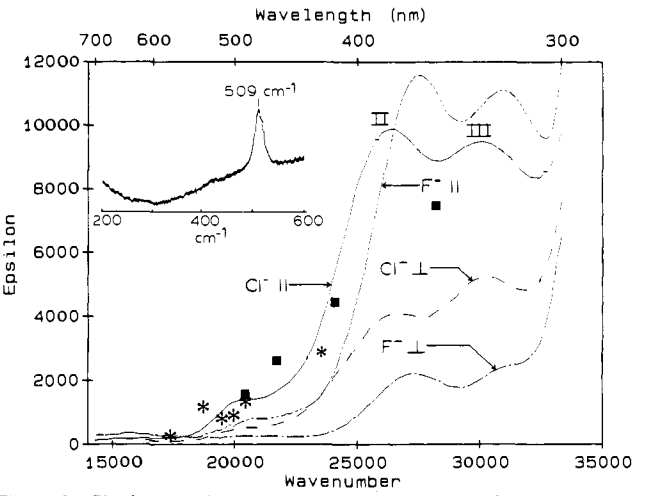

Figure 8. Single crystal UV absorbance for metCl⁻ and metF⁻Hr, polarized parallel or perpendicular to the c axis, at 298 K. Also shown (*,■) is the Raman enhancement profile of the 509-cm⁻¹ Fe–oxo stretch (inset, for 454.5-nm excitation). Two separate Raman data sets are presented, as indicated by the two symbols in the Raman profile.

The enH$_2$[(FeHEDTA)$_2$O]·6H$_2$O complex contains only the single O^{2-} bridge with a close to linear (165°) Fe–O–Fe angle.[27] The solution absorbance spectrum was previously reported[3] and shows four intense UV features, with the two lower energy features exhibiting a temperature dependence similar to that of metHr. We have obtained single crystal polarized specular reflectance data on this compound and have performed a Kramers–Kronig transformation of this data to obtain the polarized absorbance spectrum (Figure 9a). The three intense iron–oxo dimer transitions (II, III, and IV) at lower energy are found to be polarized parallel to the Fe–Fe axis, with the 344-nm band clearly the most intense. The 235-nm band is perpendicularly polarized. Perpendicular polarized spectra obtained with the electric field vector alternately in, and out of, the Fe–O–Fe plane are essentially identical.

Comparison of Figures 8 and 9a shows that the parallel polarized spectra of the tribridged and monobridged iron–oxo dimers are strikingly different. The tribridged Hr spectra show only two intense features, of similar intensity. The monobridged dimer complex shows three intense features, which decrease in intensity with increasing energy.

Exogenous Ligand Charge Transfer. As indicated in the introduction, the oxyHr and metX⁻Hr electronic absorption spectra (where X⁻ = N$_3$⁻, SCN⁻, SeCN⁻) contain new, low-energy features, which are exogenous ligand → metal charge-transfer transitions. The solution absorbance and CD and single crystal polarized absorbance data for metN$_3$⁻ and oxyHr are shown in Figures 10 and 11.

The two intense parallel polarized (Figure 11) UV bands which arise from the Fe–O–Fe unit are observed in the solution spectra (Figure 10) and can be fit to an intense negative CD feature near 380 nm and a weak positive band at about 330 nm, as in the derivatives in Figure 7. In addition, the perpendicular polarized absorbance of metN$_3$⁻Hr (Figure 11a) shows two broad, intense features near 460 and 340 nm, which must arise from azide to iron CT. (Note that the 340-nm band in ⊥ polarization peaks at an energy between the two ‖ polarized iron–oxo dimer bands, and the $I_\perp/I_\parallel$ at 340 nm is 0.39, both demonstrating that an additional exogenous ligand-to-Fe(III) CT contributes in this region). At LN$_2$ temperature, the 460-nm band begins to resolve into two transitions. The CD spectrum (Figure 10a) shows two new intense negative features, at 500 nm and about 360 nm, in both cases peaking at the low-energy side of the perpendicular polarized absorbance features. Since these signals are not present in the other met derivatives having relatively innocent exogenous

(27) Lippard, S. J.; Schugar, H. J.; Walling, C. *Inorg. Chem.* **1967**, *6*, 1825.

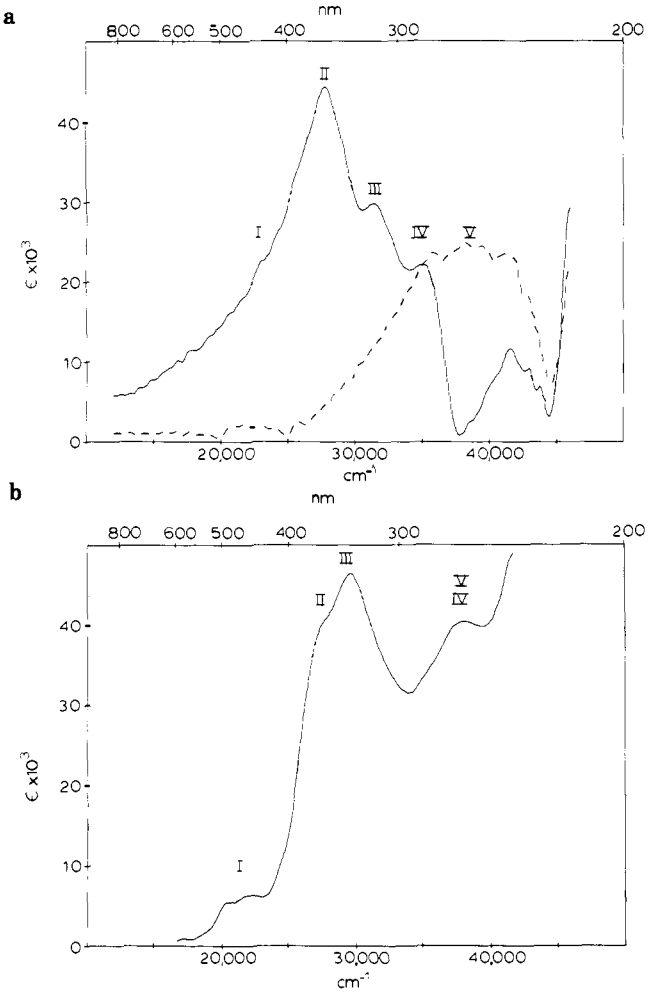

Figure 9. (a) Room temperature absorbance spectra derived from specular reflectance on single crystal of $enH_2[(FeHEDTA)_2]\cdot 6H_2O$. Data shown are polarized parallel (—) and perpendicular (- -) to the Fe–Fe axis. (b) Solution spectrum of [(Fe tri-1-pyrazolylborate)$_2$-$(OAc)_2O$]. Roman numeral labels of bands refer to the text and Table S2 in the Supplementary Material.

ligands (Figure 7), they must also be $N_3^- \rightarrow$ Fe(III) CT. The Raman profile of the Fe–N_3^- stretch clearly peaks with the CD feature (500 nm)[6b,c] (Figure 11a) and the intraazide stretch peaks at about 485 nm. Both vibrations also show enhancement into the UV, but again the peak energy is unknown. The above data require four bands arising from $N_3^- \rightarrow$ Fe(III) CT, fit as gaussians 1–4 in Figure 11 (at 20 070, 22 560, 28 010, and 30 560 cm^{-1}). There are two sets of bands (bands 1 and 2; 3 and 4), with the members of each set split by 2500 cm^{-1} and the sets split by 8000 cm^{-1}. The lowest energy band is strongest in the CD and correlates with enhancement of the Fe–N_3 stretch, while all four bands have very similar absorbance intensities.

Figure 10c shows the solution CD and difference absorbance spectra for $^1/_2$metN_3^-Hr. The absorbance and CD features clearly grow in together with addition of N_3^- to $^1/_2$met"H_2O"Hr. These data are similar in appearance to those for the metN_3^- species in Figure 10a, with bands of roughly equal intensity and nearly identical energy and the same signs in the CD. Especially note the similarity of the halfmetN_3^- absorbance spectrum with the perpendicular polarized absorbance data of metN_3^- in Figure 11a, indicating that both spectra are dominated by very similar azide-to-iron charge-transfer transitions.

The oxyHr data in Figures 10b and 11b are very similar to the metN_3^- spectra. Again the perpendicular polarized single crystal absorbance shows new broad bands at 500 and ~333 nm ($I_\perp/I_\parallel$ at 333 nm = 0.32), while the CD spectrum shows strong features at 520 and ~340 nm, both lying to the low-energy side of the absorbance bands. The Raman excitation profile of the Fe–O_2^{2-}

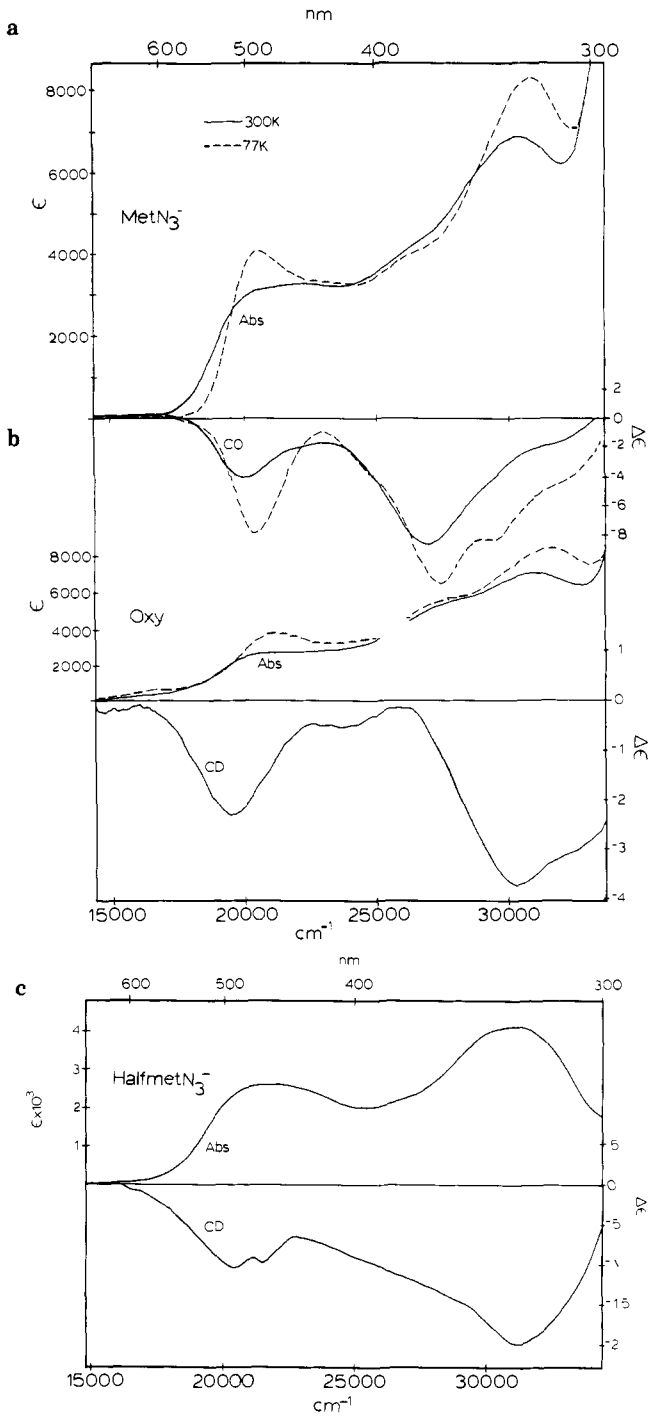

Figure 10. Solution (—, 300 K) and frozen glass (- -, 77 K) absorbance (top) and CD (lower) spectra for metN_3^-Hr (a), oxyHr (b), and half-metN_3^- (c), over the two regions on the right side of Figure 1.

stretch again peaks with the CD feature at ~520 nm.[6b] Although the exogenous LMCT spectrum is not as well-resolved as for metN_3^-, because the peroxide → Fe(III) CT bands are weaker, the data are again fit with four bands (19 100, 21 100, 29 650, ~31 800 cm^{-1}), this time having an intraset splitting of 2000 cm^{-1} and an interset splitting of about 10 500 cm^{-1}. As with the azide derivative, the lower band in each set is seen as a very intense band in the CD (which determines interset splitting), and the intraset (band 1, 2) splitting is determined from gaussian fitting of the CD and perpendicular polarized absorbance spectra. The highest energy band is obscured in absorbance by iron–oxo dimer bands and protein absorbance but can be seen in the CD as a weak negative feature at 32 000 cm^{-1} (Figure 10b).

The energies and intensities of CD and absorbance features considered above are summarized in Table IV. Also included are

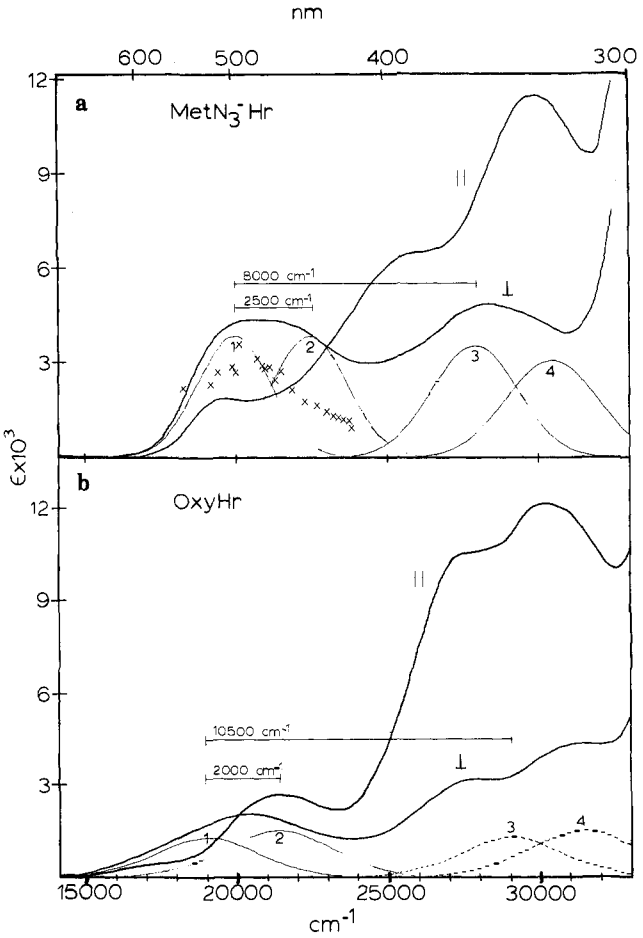

Figure 11. Single crystal absorbance data polarized parallel and perpendicular to the c (Fe–Fe) axis and Raman profile (×) for the Fe–N_3^- stretch at 376 cm^{-1} in metN_3^-Hr (a) and oxyHr (b). Also shown are gaussian resolution of the LMCT bands (perpendicular polarization), labeled as in Table IV.

the analogous data from metSCN^- and met$SeCN^-$, which have not been analyzed to the same degree.

In order to interpret the exogenous LMCT data on the protein, it is helpful to compare it to simple model compounds which exhibit analogous transitions. The absorbance spectrum of the aqueous ferric monoazide complex (Figure 12) shows a band at approximately the same position (21 700 cm^{-1}, ϵ = 3650 M^{-1} cm^{-1}) as the low-energy band in metN_3^-Hr and a much more intense band at very high energy (~38 800 cm^{-1}, $\epsilon \approx 60\,000$ M^{-1} cm^{-1}). This spectrum looks strikingly different from the data for metN_3^-Hr. Note that the experimental conditions used in Figure 12 were adjusted based on the five known sequential binding constants[28] to assure that only one N_3^- was binding to the aqueous ferric complex.

Analysis

Ligand Field Transitions. $^4T_1$ Transitions. The $^4T_1$ transitions shown in Figure 2 are not interpreted in detail due to their low intensity and general broadness. The main facility of these bands is to determine the energy of this transition (Table I), to assess the ligand field strength and allow assignment of the higher energy band as the $^4T_2$ transition. In general, it is possible to fit this region to two broad guassians. These may be associated with the $^6A_1 \rightarrow {}^4T_1$ transitions on the two different irons.

The most interesting results for the $^4T_1$ region are those of met"H_2O"Hr, where the bands are to significantly higher energy than in the other derivatives. The $^4T_1$ and $^4T_2$ transitions involve moving an electron from the antibonding e_g orbitals to the lower energy, half-filled t_{2g} level ($t_{2g}^3e_g^2 \rightarrow t_{2g}^4e_g^1$), with a stronger ligand field resulting in a lower energy transition. The ligand field strength is thus much lower in met"H_2O"Hr than in any of the other derivatives. This is consistent with the crystal structure[7] for met"H_2O" mentioned above, where one iron is found to be five-coordinate, and will be discussed in more detail in connection with the $^4T_2$ region.

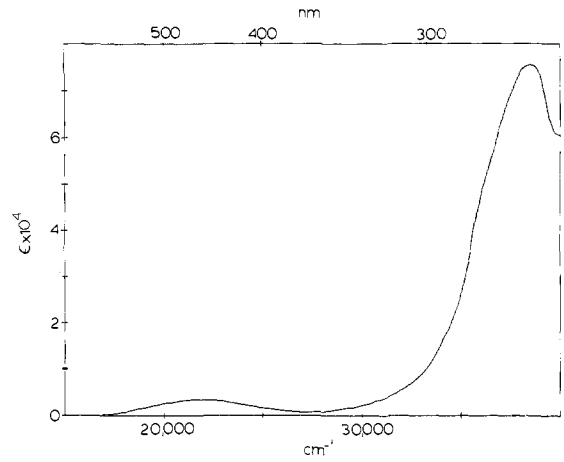

Figure 12. Solution absorbance spectrum of aqueous Fe(III) with a single azide ion bound. Data were taken at pH 0.85 and [Fe^{3+}] = 2.98 × 10^{-3} M. The iron solution was titrated with 0.2 M NaN_3 until [N_3^-] = 0.018 M.

$^4A_1$, ^4E Transitions. On the basis of energy and bandwidth considerations, it appears that the $^4A_1$, ^4E transition occurs near 480 nm for each iron. The energy of the $^4A_1$, ^4E transition is dependent on the electron–electron repulsion of the iron(III) and not on ligand field strength, as the transition is simply an electron spin flip, with no orbital change ($t_{2g}^3e_g^2 \rightarrow t_{2g}^3e_g^2$). Therefore, as the met$X^-$ derivatives have this transition occurring at very similar energies, we know their e^-–e^- repulsion, and thus covalency, is essentially constant across the series. The one exception to this is metI^-Hr, in which the transition has shifted to ~520 nm, indicating a large change in covalency upon the binding of iodide.

$^4T_2$ Transitions. The combination of variable temperature and exogenous ligand perturbations on the CD and absorbance spectra of the metHr derivatives (Figures 3 and 4) allows separation of transitions which arise from each iron at the active site. The positive CD feature near 640 nm does not shift in energy (especially clear in the gaussian fit, vide infra) upon exchange of exogenous ligands. However, the negative band to lower energy does change position (Figure 4), in a manner which is consistent with the position of the ligands in the spectrochemical series. This indicates that the negative band is due to the liganded (2-his) iron of the dimeric active site, while the low-temperature data indicate that the liganded iron distorts upon cooling. Since the energy of each CD band is constant with temperature (Figure 3), the increase in intensity and shift to lower energy of the absorbance spectrum with cooling must be due to an increase in intensity of mostly lower energy components of the band. This temperature dependence and the absorbance band shape thus indicate that several transitions are contributing in this region.

A set of gaussian bands was fit to the variable temperature absorbance and CD data, assuming bandwidths and energies are the same when measured with either technique. The bands were allowed to narrow with decreasing temperature, while the energies were held fixed. A minimum of five gaussians (bands A–E in Figure 5 and Table V) are required to simultaneously fit the room and LN_2 temperature absorbance and CD spectra in this region. A similar set of bands adequately fit the data for each metHr derivative, including the low-temperature CD of the metN_3^- species, in which these multiple transitions are clearly resolved (Figure 5a), particularly bands C, D, and E. We can assign the two high-energy bands (D and E) to the nonliganded (3-his) iron, since they are not affected by temperature and ligand field perturbations (see Table V), while the two low-energy bands (A and B), which do change, are due to the liganded (2-his) iron.

(28) Avsar, E. *Acta Chem. Scand.* **1980**, *A34*, 405.

The sign change of band C in $metN_3^-Hr$ CD (relative to the other $metX^-$ derivatives, see Figure 5b) indicates that there is also a contribution from the liganded iron in this region. The $metI^-$ and oxy derivatives exhibit behavior similar to $metN_3^-$ in this region (Figure 4b), in that band C is negative, while it is positive in all other derivatives. The explanation lies in the presence of low-energy exogenous ligand charge-transfer transitions in these derivatives, which have corresponding intense negative features in the CD. The $^4T_2$ CD bands of the 2-his iron borrow intensity from the negative CT bands, and as this mechanism involves second-order mixing, the intensity will be larger for species with lower energy charge-transfer transitions. In fact, there is a direct correlation between the energy of the lowest charge-transfer band and the rotatory strength of the lowest energy CD band, as shown in Table S1 in the Supplementary Material.

A further check on the assignment of bands is obtained from the halfmet data. Figure 6 shows the halfmet CD spectrum in the $^4T_2$ region for a number of anion bound forms. It is readily apparent that the positive feature disappears, or at least decreases greatly, upon reduction, while the negative band changes only slightly. This indicates that the 3-his iron is reduced in halfmetHr, consistent with the presence of an exogenous ligand-to-Fe(III) charge-transfer band in $halfmetN_3^-Hr$[29] (vide infra). Que et al. also showed[30] by using NMR that the liganded iron stays oxidized in halfmet.

From the total of all the data described above, it is possible to extract the positions of five $^4T_2$ bands for a number of $metX^-Hr$ derivatives. In Table V, bands A and B are due to the liganded iron, while bands D and E arise from the nonliganded iron. Both irons appear to contribute to the spectrum in the region of band C. The change in energy of bands A–C can be used to gain insight into the binding of the exogenous ligand to the 2-his iron.

The many electron wave functions for the $^4T_2$ and $^6A_1$ ferric electronic states can be written as[31]

$$\begin{aligned}
&^6A_1{:}[xy^+\,xz^+\,yz^+\,x^2{-}y^{2+}\,z^{2+}]\\
&^4T_{2(xy)}{:}[xy^+\,xy^-\,xz^+\,yz^+\,x^2{-}y^{2+}]\\
&^4T_{2(yz)}{:}(^3/_4)^{-1/2}[xy^+\,xz^+\,xz^-\,yz^+\,z^{2+}] + (^1/_4)^{-1/2}[xy^+\,xz^+\,xz^-\,yz^+\,x^2{-}y^{2+}]\\
&^4T_{2(xz)}{:}(^3/_4)^{-1/2}[xy^+\,xz^+\,yz^+\,yz^-\,z^{2+}] + (^1/_4)^{-1/2}[xy^+\,xz^+\,yz^+\,yz^-\,x^2{-}y^{2+}]
\end{aligned} \tag{1}$$

where, for example, an electron in the d_{xy} orbital with α spin is represented as xy^+. The iron–oxo bond is defined as the molecular "z" axis, as this extremely short band must produce a very strong ligand field.[32] The d_{xy} orbital will then be the most stable orbital, with the d_{xz}/d_{yz} set higher, $d_{x^2-y^2}$ 10 Dq above d_{xy}, and d_{z^2} at highest energy. The oxo bridge is actually bent toward the "x" axis, such that the projection of the oxo–Fe′ bond onto the Fe equatorial plane bisects the Fe–ligand bonds, as shown in Figure 13 (Fe≡ 2-his iron, Fe′≡3-his iron). Therefore, the d_{xz}, d_{yz} set will rehybridize into $d_{x'z}$ and $d_{y'z}$ orbitals, with the $d_{x'z}$ orbital being of higher energy.

The energies of the $^6A_1 \rightarrow {}^4T_2$ transition can then be written as in eq 2. Here E_o contains electron–electron repulsion, and Exy is the energy of the one-electron d_{xy} orbital.[33]

$$\begin{aligned}
\text{energy } ^6A_1 \rightarrow {}^4T_{2(xy)} &= \Upsilon_{xy} = E_o + Exy - Ez^2\\
\Upsilon_{x'z} &= E_o + Ex'z - (^3/_4)Ex^2{-}y^2 - (^1/_4)Ez^2\\
\Upsilon_{y'z} &= E_o + Ey'z - (^3/_4)Ex^2{-}y^2 - (^1/_4)Ez^2
\end{aligned} \tag{2}$$

Table IV. Exogenous Ligand-to-Iron Charge-Transfer Transitions

derivative	band	energy (cm^{-1})	ϵ (M^{-1} cm^{-1})
$OxyHr(HO_2^-)$	1	19100	1000
	2	21100	1000
	3	29650	<1500[a]
	4	32000?	<1500[a]
$MetN_3^-Hr$	1	20060	2000
	2	22610	2000
	3	27930	2000
	4	30500	2000
$HalfmetN_3^-Hr$		20050	1750
		22670	2000
		28100	2000
		30800	~3000
$MetSCN^-Hr$		20750	~2500
		23640	*a*
		~28500	*a*
$MetSeCN^-Hr$		19650	3400
		23640	*a*
		~28170	*a*

[a] Band position obtained from CD; therefore, ϵ is not known.

Table V. Gaussian-Resolved Bands in the $^4T_2$ Region of $MetX^-$ and OxyHr[a]

	band (cm^{-1})				
derivative	A	B	C	D	E
$MetN_3^-Hr$	13260	14280	15455	16300	17500
$MetCN^-Hr$	12900	13750	15280	16450	17500
$MetBr^-Hr$	13450	14150	15220	16050	17560
$MetOCN^-Hr$	13150	14200	15300	16500	17600
$MetI^-Hr$	12400	14300	15200	~16500	~17500
OxyHr	12500	14000	~15400	*b*	*b*

[a] Band A is fairly isolated, and thus the energy of this low-energy band is most accurately determined (±50 cm^{-1}), and band B is only somewhat less certain (±80 cm^{-1}). However, the higher energy bands are overlapping to a large degree, and thus their energies are less reliable (~±200 cm^{-1}). [b] Bands not observed due to intense, low-energy CT bands.

The lowest energy, negative CD feature (band A, Table V) is assigned as the transition to the $^4T_{2(xy)}$ state, as it involves a one-electron transition from the highest energy d orbital (d_{z^2}) to the lowest energy (d_{xy}) orbital (Figure 13). Likewise, the next two transitions are to the $^4T_{2(y'z)}$ and $^4T_{2(x'z)}$ state, respectively, and therefore the splitting between the bands B and C gives the energy splitting of the $d_{y'z}$ and $d_{x'z}$ orbitals. The energies of transitions A, B, and C can thus be used to aid the description of the bonding of each exogenous ligand, by correlating the energies of the d orbitals between derivatives. The correlation for $metN_3^-$ and $metCN^-$ is given in eq 3, where Υ_{xy} is the energy of the $^4T_{2(xy)}$ transition, and "$\Upsilon_{xyN_3} - \Upsilon_{xyCN} = 360$ cm^{-1}" is the energy difference for band A of these derivatives in Table V.

$$\Upsilon_{xyN_3} - \Upsilon_{xyCN} = (E_{oN_3} - E_{oCN}) + (Exy_{N_3} - Exy_{CN}) + (Ez^2_{CN} - Ez^2_{N_3}) = 360 \text{ cm}^{-1} \tag{3a}$$

$$\Upsilon_{y'zN_3} - \Upsilon_{y'zCN} = (E_{oN_3} - E_{oCN}) + (Ey'z_{N_3} - Ey'z_{CN}) + {}^3/_4(Ex^2{-}y^2_{CN} - Ex^2{-}y^2_{N_3}) + {}^1/_4(Ez^2_{CN} - Ez^2_{N_3}) = 530 \text{ cm}^{-1} \tag{3b}$$

$$\Upsilon_{x'zN_3} - \Upsilon_{x'zCN} = (E_{oN_3} - E_{oCN}) + (Ex'z_{N_3} - Ex'z_{CN}) + {}^3/_4(Ex^2{-}y^2_{CN} - Ex^2{-}y^2_{N_3}) + {}^1/_4(Ez^2_{CN} - Ez^2_{N_3}) = 300 \text{ cm}^{-1} \tag{3c}$$

Equation 3a shows that the negative CD band (A) falls at lower energy for the cyano complex due to a combination of three factors: the E_o term and the d_{xy} and d_{z^2} orbital energies. The d_{z^2} orbital

(29) Irwin, M. J.; Duff, L. L.; Shriver, D. F.; Klotz, I. M. *Arch. Biochem. Biophys.* **1983**, *224*, 473.

(30) Maroney, M. J.; Kurtz, D. M., Jr.; Nocek, J. M.; Pearce, L. L.; Que, L., Jr. *J. Am. Chem. Soc.* **1986**, *108*, 6871.

(31) Meltzer, R. S. *Optical Absorption of Antiferromagnetic MnF_2*; Ph.D. Thesis University of Chicago, 1968.

(32) In the well-studied vanadyl monomers[34a] and oxo-bridged chromium dimer,[34b] the metal–oxo bond length is very short, on the order of 1.8 Å, much the same as in the iron dimers. The oxo ion is a very strong field ligand and dominates the electronic structure, defining the z axis and generating large axial d orbital splittings. In vanadyl compounds, both the t_{2g} and e_g orbital sets are split by 4000–10000 cm^{-1}, and the chromium dimer also exhibits a very large splitting.

(33) Since the molecule no longer has strict octahedral symmetry, these wave functions will no longer be rigorously those given by eq 1. This could affect the absolute energy difference calculated for each orbital, but will not affect the comparison between various derivatives, and thus does not alter the conclusions drawn.

does not interact strongly with the exogenous ligand, which lies along the y axis (see Figure 13) and therefore should not affect the relative energy of band A, unless exchanging ligands distorts the oxo-bridge significantly, which is unlikely. The effect of δE_o should also be small, as the similar position of the $^4A_1,^4E$ bands in the two compounds indicates similar e^-–e^- repulsion. This then indicates that the d_{xy} orbital is lower for the metCN$^-$ complex, requiring that cyanide acts as a better π-accepting ligand than azide. The same treatment (eq 3b) for band B of the spectrum shows that the origin[35] of the red shift for the cyanide complex is the relative destabilization of the $d_{x^2-y^2}$ orbital by roughly 700 cm^{-1}, indicating that CN$^-$ is also a much stronger σ-donating ligand than N_3^-. Therefore, the lower energy of the $^4T_2$ bands for metCN$^-$Hr results simply from cyanide being a strong field ligand. The $d_{xy}/d_{x^2-y^2}$ splitting, roughly 10 Dq, is ~1070 cm^{-1} greater for metCN$^-$Hr than metN_3^-Hr, as expected based on the spectrochemical series ($Dq_{CN^-} \gg Dq_{N_3^-}$).

A parallel analysis can be performed on oxyhemerythrin, using eq 3a–c, substituting the appropriate oxyHr energies for those of metCN$^-$Hr. The same assumptions are made about e^-–e^- repulsion, as again the ligand field independent $^4A_1,^4E$ bands of the azide and peroxide derivatives are equienergetic:[11] thus $\delta E_o \approx 0$. Again the dominant ligand interaction will be with the d_{xy} and $d_{x^2-y^2}$ metal orbitals. Therefore, oxyHr has its d_{xy} orbital stabilized by roughly 750 cm^{-1} and its $d_{x^2-y^2}$ destabilized by ~400 cm^{-1}, with respect to metN_3^-. This result is surprising for two reasons. First, it indicates that oxyHr's 10 Dq splitting is about 1150 cm^{-1} larger than in metN_3^-, larger even than for metCN$^-$Hr. This is, however, consistent with the exogenous ligand charge-transfer transitions, which reflect a larger $d_{x^2-y^2}$ to d_{xy} splitting for oxyHr relative to metN_3^- (vide infra). Second, the data suggest that peroxide is a good σ-donor and is also an especially good π-acceptor or very weak π-donor, relative to the other anions studied. Since peroxide has no vacant low-lying orbitals, it must be acting as a very weak π-donor in oxyhemerythrin.[36]

Most other ligands exhibit d–d transitions which indicate they are similar to N_3^- in terms of ligand field strength (Table V). This is as expected; since the endogenous ligands remain the same, the effect of changing the single exogenous ligand should be small. However, metI$^-$Hr and met"H_2O"Hr are anomalous.

Just as in the $^4T_1$ region, the $^4T_2$ transitions are shifted to much higher energy in the met"H_2O" derivative. The low-energy, negative CD transition is observed at about 15 000 cm^{-1}, about 1800 cm^{-1} higher than in the azide derivative (Table II). Here again, the $^4A_1,^4E$ band is at the same energy, indicating that $\delta E_o = 0$. Substituting this into eq 3a gives eq 4. In this case, however, the d_{z^2} orbital should contribute to the shift. According to the

$$\Upsilon_{xyN_3} - \Upsilon_{xyH_2O} = -[(Exy_{H_2O} - Exy_{N_3}) + (Ez^2_{N_3} - Ez^2_{H_2O})] = -1800 \text{ cm}^{-1} \quad (4)$$

crystal structure of Stenkemp and co-workers,[7] one iron of met"H_2O"Hr is five-coordinate. The histidine originally trans to the oxo anion is shifted to partially fill the open coordination position, which stabilizes the d_{z^2} orbital and shifts transition A to higher energy. This picture is also consistent with the large changes that occur in the iron–oxo dimer bands (vide infra). The energy of the d_{xy} orbital should increase due to the absence of the bonding interactions of the (absent) sixth ligand, also contributing to the shift of band A. Band B from this 2-his iron cannot be assigned unambiguously, and thus no detailed information is obtained for the $d_{x^2-y^2}$ orbital.

Inserting the energies (Table V) of the metI$^-$ bands into eq 3 and making the same assumptions used above would indicate that iodide is a very strong π-acceptor (relative to the other ligands) and a somewhat weak σ-donor; contrary to what is known for iodide bonding.[37] However, the previous assumptions are clearly not valid in this derivative. First, δE_o must contribute in eq 3, since the $^4A_1,^4E$ band is shifted to lower energy in metI$^-$Hr, indicating that iodide forms a more covalent bond to the iron, as expected. In addition, the iron–oxo region between 300 and 400 nm is very different for metI$^-$ than for other derivatives, as only a single band at 340 nm is observed. This indicates that the oxo bridge has been perturbed (possibly due to the large size of I$^-$), and the other d orbitals may have shifted significantly. Solving eq 3a and 3b indicates a greater e_g orbital set splitting in the iodide complex, relative to metN_3^-. This would result from a contribution of iodide being a poor σ-donor and a destabilization of the d_{z^2} orbital due to a more linear oxo bridge. This is consistent with the iron–oxo charge-transfer data (vide infra).

Therefore the analysis of the $^4T_2$ spectral region for the methemerythrins gives results generally consistent with other spectral data and ligand bonding trends. The met"H_2O"Hr, with no exogenous ligand, and metI$^-$Hr, with very bulky ligand, both show large perturbations at the active site. The most surprising result, however, is that peroxide appears to be the strongest field ligand, with particularly weak π-donor character.

Iron–Oxo Dimer Bands. For the iron–oxo EDTA dimer model compound and for the methemerythrin complexes, most of the UV dimer band intensity is polarized roughly along the iron–iron axis, which is approximately coincident with the iron–oxo bond vector.[3,19] The FeHEDTA dimer shows three intense, parallel polarized UV transitions (bands II, III, and IV in Figure 9a), while the tribridged (bis(μ-carboxylato-μ-oxo)metHr complexes, and presumably the Lippard et al.[12a] and Wieghardt et al.,[12b] show two intense, parallel polarized bands (II, III in Figure 8) in the UV. The latter two models show an additional band to much higher energy (band V), of undetermined polarization. The EDTA dimer has a higher energy perpendicular polarized transition (band V). All these compounds also show much weaker transitions to lower energy (band I in Figure 9). These Fe–O–Fe dimer bands have been previously assigned as either simultaneous pair excitations (SPE),[3] which are two-electron processes involving d–d excitation of both irons, or alternately as oxo → Fe(III) charge-transfer transitions.[13]

If these dimer bands are SPE transitions, their energies should be approximately the sum of the energies of the two contributing one-electron (ligand field) transitions, as was previously reported[3] to be the case for the FeHEDTA dimer. In fact, however, the energy of any given dimer band must be the sum of different d–d transitions throughout the metX$^-$Hr series and in the tribridged dimers. This is inconsistent with the striking similarity of the spectroscopic features throughout this series of tribridged compounds, (including the perturbation of changing exogenous ligand in the Hr derivatives), making the assignment of these bands as SPE transitions unlikely (see Supplementary Material and Table S2).

The alternative possibility is that the dimer bands are oxo–Fe(III) charge-transfer transitions. Optical electronegativity[38] calculations can be used to predict whether oxo–Fe(III) CT bands would be in the energy region of the iron dimer bands. These are obviously crude calculations,[39] but they show that the oxo–Fe(III) CT bands should be of approximately the energy that the dimer bands occur in Hr (26 000–31 000 cm^{-1}) and the HEDTA model complexes (29 500–37 000 cm^{-1}), and, if anything, should occur

(34) (a) Lever, A. B. P. *Inorganic Electronic Spectroscopy*, 2nd ed.; Elsevier: New York, 1984; pp 384-392. (b) Dubicki, L.; Martin, R. L. *Aust. J. Chem.* **1970**, *23*, 215.

(35) Again δE_o should be insignificant based on the $^4A_1,^4E$ transition. The d_{z^2} and d_{yz} orbitals should also have small effects, as they are not directed toward the ligand.

(36) One caveat should be mentioned, with regard to the above assumptions. As the bound peroxide is thought to be protonated and hydrogen bonded to the oxo bridge,[6] this could in principle effect the energies of the other d orbitals. If the d_{z^2} orbital is thereby raised in energy, the lowest energy $^4T_2$ band will decrease in energy (eq 3a), as seen for oxyHr in Figure 4b. However, this explanation fails to explain the larger 10 Dq splitting seen in the O_2^{2-}–Fe(III) CT data.

(37) Lever, A. B. P. *Inorganic Electronic Spectroscopy*, 2nd ed.; Elsevier: New York, 1984; pp 740-753.

(38) (a) Jorgensen, C. K. Electron Transfer Spectra. In *Progress in Inorganic Chemistry*; Lippard, S. J., Ed.; Wiley-Interscience: 1979; Vol. 12, pp 101-158. (b) Lever, A. B. P. *Inorganic Electronic Spectroscopy*, 2nd ed.; Elsevier: New York, 1984; pp 218-225.

(39) See Supplementary Material for details.

to slightly lower energy. The O^{2-}–Fe(III) CT bands are expected to be polarized along the oxo–Fe bond which makes a dominant projection along the Fe–Fe vector (monobridged, $\cos^2 165° = 0.93$; tribridged, $\cos^2 130° = 0.41$). These allowed charge-transfer transitions are expected to be fairly intense, and no other parallel polarized transitions are observed below 45 000 cm^{-1} (in the HEDTA dimer). Due to the expected occurrence of oxo–Fe(III) CT bands in this region and the failure of the energy of the dimer bands to correlate to the sum of ligand field bands over a series of Fe–O–Fe complexes (as would be required for SPE transitions), we strongly favor the assignment of these intense, parallel polarized, "UV dimer bands" as oxo → iron(III) CT transitions.

In analyzing the oxo–Fe(III) CT spectrum we focus on an energy level scheme for a $Fe–O^{2-}$ unit and therefore assume weak interaction between irons (as is consistent with the two Fe(III)'s being antiferromagnetically coupled). To a first approximation, the addition of the second iron simply modifies the valence orbital scheme of the bridging oxo ligand. We first consider a linear Fe–O–Fe unit with the other ligands treated as σ donors, as in Figure 14a. The site symmetry of the iron is thus C_{4v}. The d-orbital splittings result dominantly from interaction with the oxo orbitals and have been described in Figure 13. The oxo orbitals split into p_z (a_1), which is stabilized by the strong bonding interaction with Fe d_{z^2}, and the p_x, p_y (e) set at lower binding energy. All transitions to the metal d orbitals which originate from the oxo e(p_x,p_y) set are group theoretically allowed, but only the metal e(d_{xz},d_{yz}) orbitals have overlap (π) with the oxo e set and thus should have significant CT transition intensity (polarized ∥ to the Fe–O bond).[40] Transitions from oxo e orbitals to the other metal orbitals will be weak. Transitions arising from the O^{2-} p_z orbital are group theoretically allowed to the Fe e(d_{xz},d_{yz}) and $a_1(d_{z^2})$ orbitals in absorbance and to the e(d_{xz},d_{yz}) and $a_2(d_{x^2-y^2})$ in CD and are forbidden to the b_1 and b_2 orbitals. The O^{2-} p_z to Fe(d_{z^2}) a_1 transition should produce an intense parallel polarized absorbance band due to large σ orbital overlap but should lie about 20 000 cm^{-1} higher[41] in energy than the O^{2-} e(π) → Fe e(d_{xy},d_{yz}) transition. Therefore, this model predicts a fairly intense (π) transition to low energy (~28 000 cm^{-1} from optical electronegativity), a very intense (σ) transition at high energy (~50 000 cm^{-1}) (both parallel polarized), and perhaps some weak transitions to other Fe d orbitals which have little direct overlap but gain intensity through higher order mixing with these σ and π bands.

Figure 14 (parts b and c) presents the perturbation of these orbitals and the associated transitions when the Fe–O–Fe angle is decreased from 180° to the geometry of the tribridged dimers. The lowered symmetry energy level scheme is similar to Figure 14a, except the degenerate levels split with an energy difference that increases as the angle decreases from 180°. The energies of the Fe $d_{y'z}$ and oxo $p_{y'}$ orbitals do not change with bending nor does their overlap. However, the Fe $d_{x'z}$ orbital will increase in energy since it begins to interact in a σ manner with O p_z as the Fe–O–Fe angle decreases, while d_{z^2} decreases in energy as its σ-overlap with O p_z decreases. The oxo $p_{y'}$ and p_z orbitals converge to an intermediate energy, becoming degenerate when ∠Fe–O–Fe = 90° (Figure 14c). Therefore, as the oxo bridge is bent, the oxo e(p_x,p_y) → Fe e(d_{xz},d_{yz}) transition splits, with the $p_{x'}$ → $d_{x'z}$ transition moving to higher energy and losing intensity, as the π overlap decreases. The O p_z → Fe $d_{x'z}$ transition also becomes allowed (in the lowered symmetry), gaining intensity and shifting to lower energy as ∠Fe–O–Fe decreases and the orbital overlap increases. The p_z to d_{z^2} transition loses some intensity and decreases in energy but should still be a very high-energy transition.

Thus in a bent oxo-bridged ferric dimer, we expect a very high-energy (>45 500 cm^{-1}), very intense band and three fairly intense bands at lower energy. In nearly linear cases, the three lower energy bands should be of decreasing intensity with increasing energy. This predicted spectrum is observed in the $enH_2[(FeHEDTA)_2O]\cdot 6H_2O$ (Fe–O–Fe angle = 165°) single crystal polarized data (25 000–38 000 cm^{-1} in Figure 9a). These

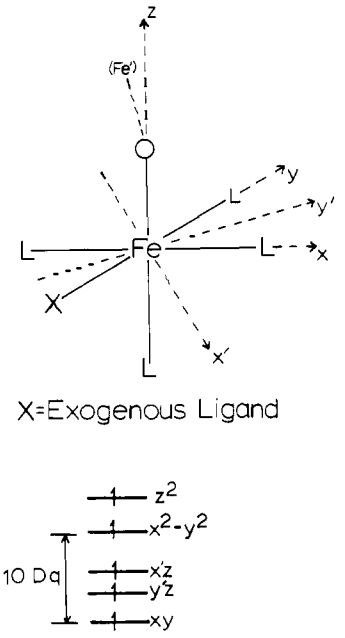

Figure 13. d orbital splitting of Fe(III) in metX⁻Hr showing axes and geometry described in text.

three bands (II–IV) are polarized parallel to the Fe–Fe axis, as expected from Figure 14. A higher energy band, at about 42 000 cm^{-1}, is very broad and dominantly perpendicular polarized. This polarization and the presence of a band of very similar intensity and energy in the spectrum of the monomer[3] allow assignment of this high-energy band to L → Fe(III) CT from the EDTA carboxylato groups. The higher energy region where the intense oxo p_z → Fe d_{z^2} transition is expected cannot be probed, due to intense absorbance of other groups in the complex.

As the Fe–O–Fe angle approaches 90°, the two higher energy, oxo π derived bands should merge, resulting in a spectrum which shows two similarly intense transitions (see Figure 14c). The tribridged dimer systems should approach this situation, having an Fe–O–Fe angle near 130°. MetX⁻Hr derivatives do exhibit two intense, parallel polarized bands below the protein absorbance cutoff, and the tribridged model compounds show two bands of very similar energy and intensity. A weaker, higher energy band (~38 000 cm^{-1}) present in these models is of an energy where carboxylate → Fe(III) CT is expected[42] but polarized data are required for a definitive assignment.

In the HEDTA dimer another much weaker band (band I in Figure 9a) is seen as a low-energy shoulder on the intense UV features and is resolved in the low-temperature (glass) spectrum[3] as a peak at 24 800 cm^{-1}. Similar weak, lower energy absorbance bands (bands I in Figure 9b) are observed between 19 000 and 23 000 cm^{-1} in the tribridged dimers (including Hr), but this region is complicated in both systems by the presence of ligand field bands of similar intensity. The Raman excitation profile[12a,c,26b,c] on the Lippard et al. and Wieghardt et al. models indicate features near 405 nm (24 700 cm^{-1}) and 525 nm (19 000 cm^{-1}); both of which correspond to weak shoulders in the absorbance spectrum. Similar features are seen in the Raman profile of hemerythrin[6,26c] (see Figure 8a).

Since the intensity of the $^4T_2$ and $^4T_1$ transitions in the iron–oxo dimer compounds is about two orders of magnitude greater than that expected for mononuclear octahedral Fe(III), one must consider whether these weak, low-energy shoulders (showing the enhancement) could be Fe(III) ligand field bands.[43] However, since only the iron–oxo stretch is enhanced, these two transitions

(40) $I_{CT} \propto (S/R)^2$, where R is the ligand-iron distance and S is the overlap of donor and acceptor orbitals involved in the CT process.

(41) This should be roughly the sum of the oxo σ–π splitting (about 10 000 cm^{-1}) and 10 Dq for Fe(III) (about 13 000 cm^{-1}).

(42) The oxo–Fe(III) σ transition should be at higher energy (>45 000 cm^{-1}) and greater intensity than the π transitions.

(43) The extra absorbance intensity is obtained by mixing with the intense near-UV oxo bonds, resulting in intense parallel polarized ligand field bands.

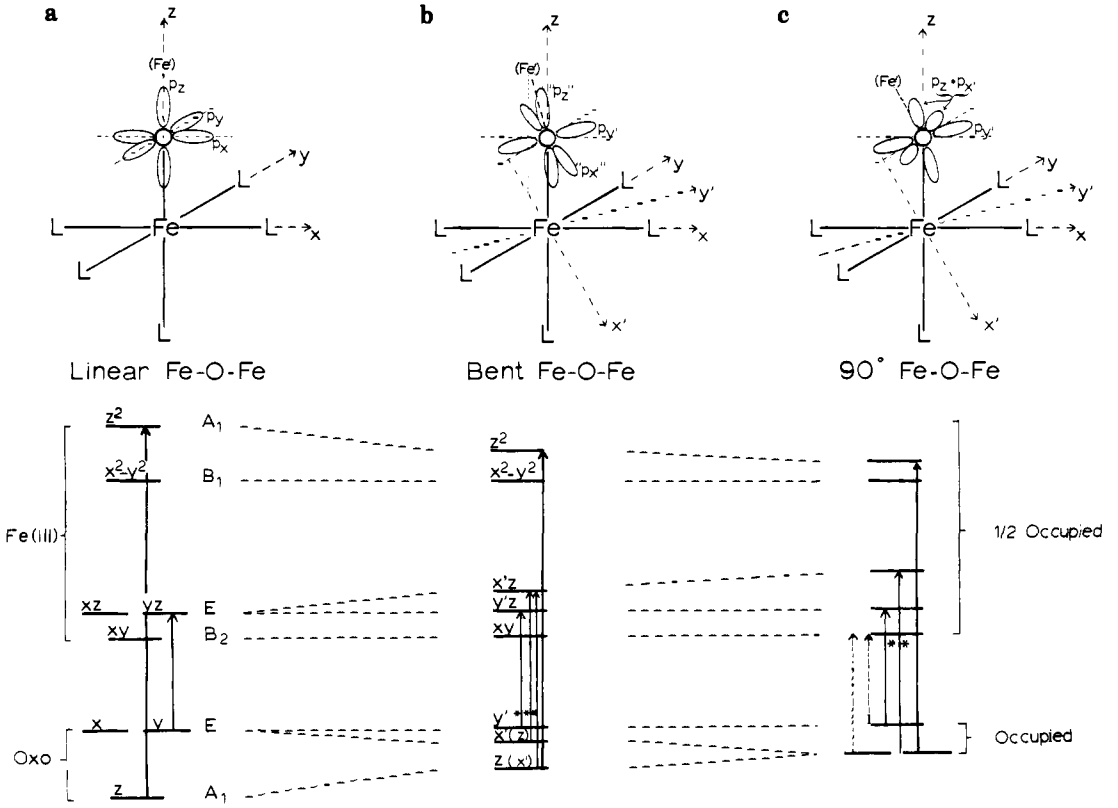

Figure 14. (a) Energy level diagram for Fe(III)-oxo bond in linear Fe–O–Fe geometry, (b) when the bridge is bent, and (c) when the bridge angle is 90°. Transitions allowed by group theory and having reasonable overlap (therefore significant intensity) are shown as vertical arrows. *'s represent bands II, III, and IV in Figure 9. Dotted arrows represent weak, formally forbidden transitions. See text for discussion.

where the Raman intensity profile peaks are assigned to be oxo–Fe(III) CT bands and not ligand field transitions.[44] Two explanations for these additional low-energy oxo CT features should be considered.

The first involves the effects of electronic coupling of CT transitions to two irons at the active site. Although the two irons are not equivalent in the protein, they are symmetry related in the model complexes, so the two visible (and UV as well) transitions cannot simply arise from transitions to inequivalent irons. However the presence of two irons will split each single iron CT transition into symmetric and antisymmetric combinations. From either a group theoretical approach or transition dipole moment vector coupling approach,[45] it is possible to predict the polarizations and relative intensity of these extra bands. A vector coupling model predicts that each of the intense parallel polarized UV features will have a corresponding weaker, perpendicular polarized (in the Fe–O–Fe plane) transition (arising from the symmetric combination). The intensity of the perpendicular bands depends on the bridge angle ($I_\perp/I_\parallel \propto (\sin 180 - \theta)^2$), having no intensity in the linearly bridged dimers and becoming as intense as the parallel component when ∠Fe–O–Fe(θ) = 90°. Since no dominantly perpendicular bands are identified below 30 000 cm^{-1} in either the protein or the EDTA model (Figures 8 and 9a), no bands can be unequivocally assigned to this dimer mechanism.[46]

The alternative explanation is that the weak low-energy bands in the dimer complexes are simply forbidden oxo–Fe(III) CT bands (O $p_{x'} \rightarrow$ Fe d_{xy}, O $p_{y'} \rightarrow$ Fe d_{xy}, dotted in Figure 14c) with little overlap and thus low intensities. These gain some intensity by mixing with the intense transitions as the symmetry is lowered. The model in Figure 14b predicts that the lowest energy CT band will be the weak, perpendicular polarized O $p_{y'} \rightarrow$ Fe d_{xy} transition. One would initially expect the O $p_{x'}$ to Fe d_{xy} transition to be of similar energy to the much more intense O $p_{y'} \rightarrow d_{yz}$ transition and thus not be observable. However, the O $p_{x'}$ to Fe d_{xy} transition may be lower energy than predicted by the one-electron orbital scheme, due to dimer interactions (i.e., the presence of excited state exchange interactions).[47] On the basis of the available spectral results it is not possible to make a convincing choice between these two alternatives; however, detailed single crystal spectral and theoretical studies of model complexes in this energy region should allow a definitive assignment.

Exogenous Ligand-to-Metal Charge Transfer. The exogenous ligand-to-metal charge-transfer (ELMCT) bands have been fairly accurately assigned for all ligands studied, using a combination of polarized single crystal absorbance, solution CD, and absorbance spectroscopies, all at variable temperature, and resonance Raman spectroscopy. These bands are located at energies close to those expected from previous studies on aqueous ferric complexes, as discussed by Klotz and co-workers.[11] However, the low-energy charge-transfer bands of certain ligands have now been studied in detail to yield insight into exogenous ligand bonding to the iron site. In particular, the complexes of azide and peroxide ligands are analyzed below.

The azide and peroxide derivatives shown in Figures 10 and 11 both show two low-energy features (bands 1 and 2, in gaussian resolution) of equal intensity in absorbance, the lowest of which (band 1) shows strong CD and enhances the metal–ligand and intraligand vibrations in the Raman.[6b,c] In addition two bands appear at higher energy (bands 3 and 4) with (approximately) the same intensity as the lower energy bands. Bands 1 and 2 are split by the same amount as bands 3 and 4, while the band 1–3 splitting is much greater. These spectra are strikingly different from that of the aqueous ferric monoazide complex (Figure 12).

(44) Mixing of the oxo charge-transfer transitions could be sufficient for weak enhancement of the oxo vibrations in the Raman spectra. However, excitation of the d–d bands would enhance other metal ligand vibrational modes, as the excited state geometries for these transitions involve Franck-Condon distortions of all metal-ligand bonds.

(45) Eickman, N. C.; Himmelwright, R. S.; Solomon, E. I. *Proc. Natl. Acad. Sci. U.S.A.* **1979**, *76*, 2094.

(46) It is conceivable that the two low-energy bands giving rise to Raman enhancement in the tribridged dimer models and hemerythrin are the perpendicular components of the dimer bands but are very weak (for θ = 130°, $I_\perp < {}^1/_5 I_\parallel$), such that they are obscured by ligand field transitions in the hemerythrin (perpendicular) spectrum.

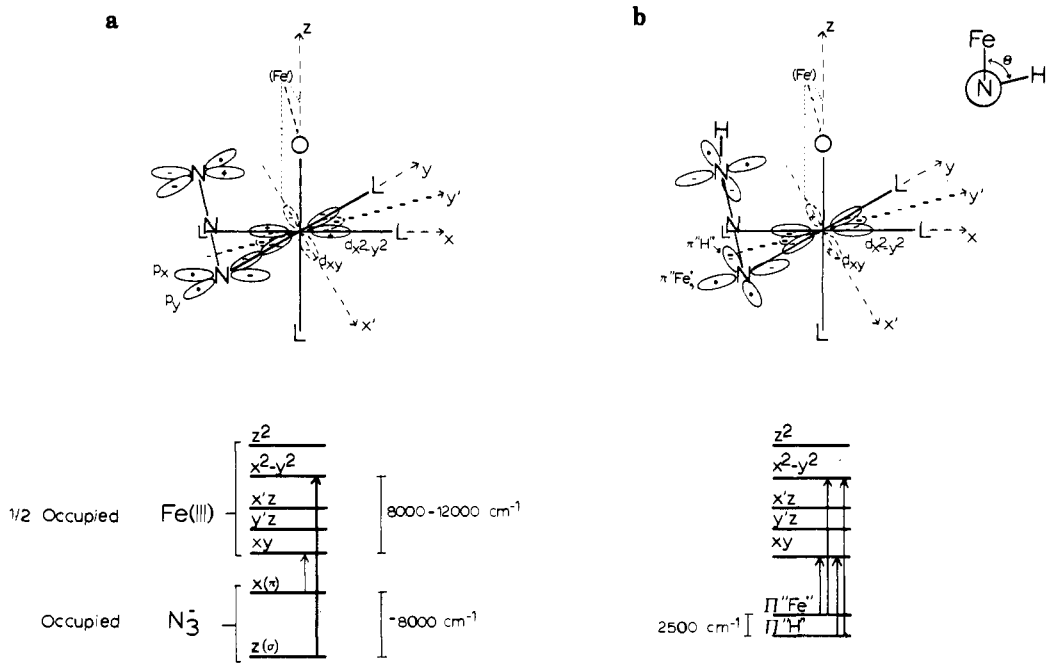

Figure 15. Energy level diagram for azide interacting with an Fe(III)–O^{2-} unit: (a) free azide and (b) protonated azide. π "Fe" and π "H" represent the azide HOMOs which interact most strongly with the iron and proton, respectively. See text for details.

The thiocyanato complex also exhibits features which are readily distinguishable from the N_3^- and O_2^{2-} derivatives. There are again two low-energy bands, but here the higher energy of the two has the more intense CD spectrum and increased Raman enhancement. Again there is a higher energy band, but the data do not allow the resolution and identification of separate components.

The features can be interpreted in terms of the model of exogenous ligand binding given in Figure 15. The azide binds cis to the oxo ion with NNN aligned roughly parallel to the iron–oxo bond vector.[7] The iron–oxo bond generates the d orbital splitting in Figure 13, to which the valence azide orbitals must be added. The azide ion has a filled degenerate π nonbonding set (HOMO): essentially the lone pair electrons filling the p_x,p_y orbitals on the two end nitrogens. This degeneracy is split when the azide ion interacts with the metal. When a proton binds to N_3^-, one Np_π orbital interacts with the H_{1s} orbital and is stabilized by about 12 000 cm^{-1} relative to the other nonbonding Np orbital.[48] Azide binds to hemerythrin with a Fe–N–N angle of 112° and should interact much as with the proton but with weaker σ-bonding interaction. We would also expect the remaining N_3^- π orbital to be somewhat stabilized, due to its π-bonding interaction with the d_{xy} orbital (Figure 15a). There will thus be a lower energy transition between the Np_π and d_{xy} orbitals with significant intensity (due to π-overlap), and the more stabilized p_σ orbital will give rise to a higher energy, very intense transition to $d_{x^2-y^2}$, due to the strong σ-overlap. Thus the σ/π splitting should be less than in HN_3, here about 6000–8000 cm^{-1}, and the $d_{xy}/d_{x^2-y^2}$ splitting should be about 10 *Dq*, approximately 10 000–13 000 cm^{-1} for Fe(III). Therefore we expect a low-energy band and a very intense high-energy band about 16 000–20 000 cm^{-1} to higher energy. This predicted N_3^-–Fe(III) CT spectrum is observed for the aqueous ferric azide complex in Figure 12 but is very different from the metN_3^-Hr data in Figures 10 and 11.

Two observations aid in assigning the electronic transitions responsible for the azide-to-iron (III) CT bands. The first is the fact that the splitting between the two lower energy transitions is equal to that in the higher energy pair. These splittings imply that the low- and high-energy sets of bands either originate from, or end at, the same two orbitals. The second observation is that the CD and absorbance spectra for halfmetN_3^- are very similar to those of metN_3^- (Figure 10a,c). Therefore energies of the d orbitals and their interactions with the azide orbitals do not change significantly upon forming halfmet.

For various reasons,[49] the oxo bridge is not believed to be present in halfmetN_3^-Hr and its most likely replaced with a hydroxo bridge. Since the d_{z^2}, $d_{x'z}$, and $d_{y'z}$ orbitals interact strongly with the oxo anion (Figure 13), one would expect them to be of significantly lower energy in halfmetHr (i.e., split by the much weaker field OH^-), and N_3^- to Fe(III) CT bands to these levels would thus change significantly in the halfmet. As no such change occurs, the four observed charge-transfer bands in metN_3^-Hr (and oxyHr) must terminate on the d_{xy} or $d_{x^2-y^2}$ metal orbitals. These two metal orbitals are split by 10 *Dq*, which is typically 10–13 000 cm^{-1} for octahedral Fe(III) with an N or O ligand set. This is approximately the splitting between the lower and higher sets of bands (8000 cm^{-1}) but is much larger than the 2500 cm^{-1} splitting within the sets (i.e., band 1–2). Therefore, the low-energy bands arise from transitions terminating on the d_{xy} orbital, while the high-energy bands end on $d_{x^2-y^2}$, and the 2500-cm^{-1} splitting corresponds to the azide p_σ/p_π orbital splitting. This p orbital splitting and the equal band intensity pattern are not consistent with a π/σ arrangement for azide binding (Figure 15a) and indicate an unusual binding mode.

This difference between this Fe(III)–N_3^- bonding model in Figure 15a (and the corresponding N_3^- CT spectrum in Figure 12) and the metN_3^- spectral data in Figures 10 and 11 should result from mixing of the azide valence p orbitals and would occur if a strong bonding interaction was present between the azide and an additional atom at the active site. If a proton is bound to the terminal nitrogen at a nonzero dihedral angle ($\theta > 0°$ in Figure 15b) with respect to the iron, the azide p orbitals will be mixed and rotated with respect to the N–Fe bond. These new hybrid orbitals will no longer be strictly π or σ with respect to the metal. Both will now overlap with the Fe d_{xy} and $d_{x^2-y^2}$ orbitals, and thus the intensity of the LMCT bands will be spread over all four transitions. In addition, since both p orbitals will now have strong bonding interactions with either the metal or the proton, the "π/σ" splitting will be much smaller.

(47) Desjardins, S. R.; Wilcox, D. E.; Musselman, R. L.; Solomon, E. I. *Inorg. Chem.* **1987**, *26*, 288.

(48) (a) Lee, T. H.; Colton, R. J.; White, M. G.; Rabalais, J. W. *J. Am. Chem. Soc.* **1975**, *97*, 4845–4851. (b) Bonaccorsi, R.; Petrongolo, C.; Scrocco, E.; Tomasi, J. *J. Chem. Phys.* **1968**, *48*, 1500–1508.

(49) The most convincing[30] being a much smaller exchange coupling of $J \approx -15$ cm^{-1}.

The resonance Raman excitation profile shows that the met-al–azide stretch is in resonance with the lowest energy charge-transfer transition, indicating that this transition results in an excited state with a significantly distorted Fe–N_3^- bond, while the higher energy band 2 does not. Since both transitions are to the d_{xy} orbital, the lower energy band must originate from the azide p orbital which is most strongly bonding to the metal. This at first is unexpected, as the more strongly bonding orbital should be most stabilized. The data thus indicate a stronger bonding interaction occurs at the terminal nitrogen, as would be the case with a protonated azide.

Because the oxyHr spectrum is so similar to the metN_3^- data, it appears that the same type of interaction as in Figure 15b is present with the peroxide ligand as well. In fact, the Raman vibrational frequencies in oxy are shifted when H_2O is replaced by D_2O. This has been interpreted[6] as showing that peroxide is protonated and hydrogen bonded to the oxo bridge. This is consistent with the low Fe–O–Fe stretching frequency in the Raman, the lower exchange coupling, and the small shift in the oxo–Fe CT bands in oxyHr relative to the met derivatives. The proton will again form a stronger bond with the peroxide than will the metal, causing the mixing that results in small σ/π splitting and equal intensities of the absorbance bands. The equal intensities observed indicate similar overlaps of each p orbital with the metal d electrons, calling for a dihedral angle (θ) nearing 90°. The stronger bonding with the proton also explains the enhancement of the Fe–O_2^{2-} stretch by excitation only into the lower energy CT band 1.

The thiocyanato complex shows different behavior, especially in the Raman excitation profile. Here the second charge-transfer band clearly enhances the vibrations more than the low-energy band. The absorbance data do not allow clean resolution or assignment of the bands, so a detailed analysis is not possible. However, it is apparent that the SCN^- anion is not protonated when bound to the protein, as any interaction with the thiocyanate ion must be weaker than the Fe–N bond.

The above assignments show that the $d_{xy}/d_{x^2-y^2}$ splitting in metN_3^-Hr is about 8000 cm^{-1}, while the equivalent splitting in oxyHr is 10 500 cm^{-1}. This is consistent with the $^4T_2$ absorbance band analysis described in the ligand field section. We also see that the p_σ/p_π splitting, although small in both derivatives, is smaller for peroxide than for azide and is the same in halfmetN_3^- as for metN_3^-Hr.

Discussion

The ligand field spectrum of metX^-Hr gives information about the difference between the electronic structure of the two iron atoms at the site and on the bonding of exogenous ligands. Binding of various exogenous ligands dominantly perturbs the 2-his iron, while binding of anions has little effect on the spectrum of the 3-his iron, other than small intensity changes. Therefore, any electronic changes are not strongly communicated through the oxo-bridge upon ligand binding, and, at most, small geometrical changes occur at the 3-his Fe(III). In addition, the reduction of met to halfmetHr clearly reduces the 3-his iron, with the 2-his iron retaining roughly the same ligand field spectrum.

The large difference in the strength of the ligand fields at the two irons is surprising, particularly since the ligands on each are essentially identical; the only difference is the exogenous ligand on the 2-his iron replaces the third histidine on the 3-his iron. The exogenous ligand has a similar or weaker ligand field than histidine, and so an alternative explanation must be found for the strong ligand field of the 2-his iron. Since the oxo-bridge makes the dominant contribution to the electronic structure of the active site, relatively small changes in its structure will result in significant changes in the ligand field strength at the site. An asymmetric oxo-bridge, with a shorter bond to the 2-his iron, would generate the observed differences (including that seen in Mössbauer spectroscopy[2]). The crystal structure[7] does in fact suggest that the oxo ion lies closer to the 2-his iron. At the present 2.0 Å resolution of the structure, short bond distances like the 1.8 Å Fe–O bond are unreliable, but the same result is exhibited by all nonsymmetry related iron dimer sites. EXAFS data[50] do not indicate this asymmetry, however, so any differences in bond length are <0.1 Å.[51]

The ligand field spectral region also gives information on the bonding of exogenous ligands through changes in features relating to the 2-his iron. Most of the metX^-Hr derivatives show only slight differences from one another, as expected, since only one ligand of six is varied. Cyanide, "aquo", iodide, and peroxide complexes are exceptions.

Analysis of the CD and absorbance bands of metCN^-Hr shows that CN^- acts as a much better σ-donor and a better π-acceptor than the other ligands, much as is expected of the very strong field cyanide ligand based on inorganic model complexes. The met"aquo"Hr spectrum apparently shows a very weak ligand field, which is consistent with an open coordination position at the 2-his iron, as shown in the crystal structure.[7] This is contrary to the X-ray absorption edge data[52] which were interpreted in terms of two six-coordinate irons. The distortion of the histidine ligand trans to the oxo group stabilizes the d_{z^2} orbital and markedly blue shifts the lowest energy component of the $^4T_2$ band, as the data in Figure S1 of the Supplementary Material reflect. The anomalous spectral data for metI^-Hr probably result from distortion of the site due to the large size of the iodide ion.

The ligand field spectrum for oxyHr indicates that peroxide behaves as a strong field ligand. This arises from a somewhat better σ-donor, and much weaker π-donor interaction relative to other ligands. The O_2^{2-} – Fe(III) CT spectrum also reflects a very large 10 *Dq* splitting for oxyHr, which is not expected based on the spectrochemical series. The origin of this strong field behavior appears to relate to protonation of the peroxide ligand. With the proper dihedral angle θ (Figure 15b), the proton will shift electron density from the peroxide p orbitals that interact with "π-bonding" metal d orbitals and produce very weak π-donor character relative to other exogenous ligands (and that expected for peroxide).

A final comment on the ligand field transitions concerns the origin of their high intensities, which has been suggested to arise from exchange coupling in the dimer site, which would remove the spin forbiddeness.[13a] In the dimer, spin-allowed transitions would arise from the excited $S = 1$ (or 2) total spin components of the exchange coupled ground state and terminate on triplet (or quintet) excited substrates produced by coupling the sextet ground state on one iron with an excited quartet state on the other.[3] This mechanism requires a loss of intensity as the temperature is decreased, since at low temperatures only the ($S = 0$) spin singlet ground state is occupied, and, since there is no (one electron) singlet excited state, the transition is spin forbidden. This effect is observed in the $^4T_1$ transition of the HEDTA dimer complex, where most of the room temperature intensity in the parallel polarized spectrum is cooled out.[13a] Alternatively, this effect is not seen in the $^4T_2$ transition in Hr, since the intensity actually increases as the temperature is lowered (Figure S2 in the Supplementary Material). Therefore, the large intensity in Hr d–d bands does not arise from an exchange mechanism, but rather from a large static distortion which increases with decreasing temperature. Since the ligand field bands are parallel polarized (see Figure S2), this intensity is stolen from the intense, low-energy oxo bands by low symmetry mixing.

The intense UV absorbance features in hemerythrin and the iron–oxo dimer model complexes are assigned as oxo–Fe(III) CT bands based upon a systematic comparison of ligand field and dimer band energies in the tribridged species, plus consideration of the expected energies of charge-transfer bands. The appearance of the oxo–Fe(III) CT bands in absorbance depends on the bond angle of the oxo-bridge, as seen by comparison of the nearly linear

(50) Co, M. S. *X-ray Absorption Spectroscopy of Hemocyanin and Hemerythrin*; Ph.D. Thesis, Stanford University, 1983.

(51) Other explanations, such as a difference in covalency at the two irons or grossly different bond lengths or angles, are inconsistent with $^4A_1$,^4E bands or the published crystal structures.

(52) Sheriff, S.; Hendrickson, W. A.; Smith, J. L. *Life Chem. Rep.* **1983**, Suppl. *1*, 305-308.

FeHEDTA dimer (Fe–O–Fe angle = 165°) with the tribridged site of the protein and models (Fe–O–Fe angle = ~130°). Significant σ-bonding character is lost from the oxo p_z–iron d_{z^2} orbital overlap upon bending. Some σ overlap is regained between p_z and d_{x^2}, but there appears to be some net loss in bond strength. This is reflected in the decrease in the energy and average splitting of the oxo charge-transfer bands. Although generally there is no firm correlation between bridge angle and exchange coupling to iron–oxo dimers,[53] this is probably due to different ligation and geometry at the iron. Two recent studies[54,55] have shown such a correlation. Murray et al. reported a $[(FePc)_2O]$ dimer which exists in two crystalline forms that have very different bridge angles.[55] The linear dimer shows $-J \approx 190$ cm^{-1}, while the bent structure ($\angle$FeOFe = 140°) shows $-J \approx 120$ cm^{-1}, consistent with a change in the electronic structure of the bridge upon bending. The study[54] by Holm and co-workers gave parallel results, with $[Fe(salen)]_2O$ and $[Fe(3\text{-}t\text{Busaltmen})]_2O$ having bridge angles of 145° and 173° and $-J = 183$ and 208 cm^{-1}, respectively. The Fe–O distance does not vary in either of these studies.

The large changes in the oxo–Fe(III) CT transitions indicate significant change in the iron–oxo bond with angle, and this change in bonding could lead to changes in the chemistry of the oxo-bridge. The bent bridge in the tribridged Hr site would tend to raise the pK_a of the bridging oxygen atom (by stabilizing the hydroxide bridge relative to the oxo-bridge), thus strengthening the hydrogen bond in oxyHr. This effect could contribute to the removal of the proton from the peroxide in order to facilitate its reversible loss as dioxygen. This should be a synergistic process where transfer of the proton to the oxo ion makes peroxide more π-donating and forms the hydroxide bridge which stabilizes the Fe(II) oxidation state. It is also possible, however, that the acetate bridges simply serve to stabilize the hydroxide bridge in deoxyHr,[56] thereby preserving a superexchange pathway for the two-electron transfer from the binuclear iron sits to dioxygen, which is bound at one iron.

This assignment of the oxo charge-transfer spectrum also provides a probe into perturbations in the structure of the bridge among different binuclear ferric proteins. The electronic spectrum of the binuclear iron protein ribonucleotide reductase is nearly identical with that of hemerythrin in the near UV (oxo CT) region[57] and therefore requires an oxo-bridge with a similar angle. It is likely that carboxylato or other similar bridges are present to stabilize this small oxo-bridge angle, as model complexes with similar small Fe–O–Fe angles are all tribridged structures. On the other hand, the spectrum of the purple acid phosphatases (including uteroferrin) and methane monooxygenase show only a weak band in the 320-nm region,[58] indicating either a more linear oxo bridge or an alternative bridging ligand.

Three Hr derivatives (with O_2^{2-}, OH^-, and F^-) show the lower energy band II, assigned as the oxo $p_y \rightarrow$Fe(III) d_{yz} transition, blue-shifted in relation to the other metX$^-$ species. The first two of these have been implicated in hydrogen bonding to the bridge,[6] which could certainly change the energy of the oxo p_y, orbital, and thus change the energy of this transition. It is interesting that fluoride shows a similar effect in the oxo CT bands. These effects have previously[11] been interpreted as indicating multiple F^- binding but may, in fact, involve interactions with the bridge. Alternatively, it should be noted that metN$_3^-$ Hr does not show this effect in its oxo CT spectrum.

The exogenous ligand-to-metal charge-transfer region is most informative as to the nature of the electronic structure of the peroxide–iron bond in oxyhemerythrin. The small "σ/π" splitting and roughly equal intensities[59] are observed due to an additional strong interaction of the ligand, consistent with the protonation of the peroxide as indicated by the Raman data. This is also consistent with the unusually weak π-donor character of peroxide, as displayed in the $^4T_2$ region of oxyHr.

The absorbance spectrum and resonance Raman profile for the metN$_3^-$Hr derivative are strikingly similar to the oxyHr data and are consistent with azide also having another strong interaction in addition to binding to the iron. This gains some support from the kinetics of azide binding to the met site. Wilkins and co-workers showed[60] azide binds at about the same rate as most other anions, while the off rate is several orders of magnitude slower than for most anions, and speculated that azide was bridging the binuclear site. Although it is now clear that the anion is not bridging the irons, the idea of another interaction with the azide is consistent with the absorbance and kinetic data. Variable pH kinetic data[60] showed no evidence for a change in protonation of the azide in the range studied (pH 4–10).

Although the above is consistent with azide also binding protonated to the active site, Raman data on the metazide derivative show no shift (within the ~1 cm^{-1} experimental resolution) upon deuteration for any vibration.[61] However, the intraperoxide and metal–ligand stretching vibrations in oxyHr shift by very small amounts (in different directions) upon D_2O substitution, due to opposing contributions of the weakened hydrogen bond and the mass effect.[6] In addition, the asymmetric stretching vibration of H_2O_2 does not shift upon deuteration,[62] while that of HN_3 moves only 1 cm^{-1} and that in the opposite direction expected for the mass effect.[63] Therefore, the lack of Raman shift upon deuteration of metN$_3^-$Hr is inconclusive.

There is evidence[64] that azide binds to some protein sites as HN_3. Although azide bound to Fe(III)(aq) would normally be expected to have a $pK_a < 4$, the crystal structure shows the hemerythrin active site pocket to be very hydrophobic,[65] which could stabilize the protonated azide (peroxide and azide have higher pK_a's than the other exogenous anions studied). This could also lead to the slower off rate for the neutral HN_3 compared to the anionic exogenous ligands.

The above results, together with our earlier report showing that deoxyhemerythrin contains one six-coordinate and one five-coordinate iron bridged by hydroxide,[56] lead us to the model shown below for the reversible oxygen binding in hemerythrin consistent

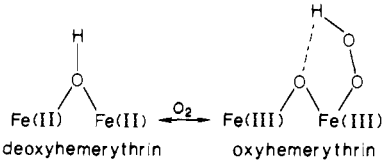

with that proposed before.[6] The protonation of the peroxide significantly changes the nature of its bonding to the Fe(III), making this ligand less likely to donate electrons back to the iron. The hydrophobic nature of the active site pocket appears to strongly stabilize this protonated structure. At the same time, the hydrogen bond[6] will deter the undesirable loss of HO_2^-, thereby preventing the irreversible production of metHr. All the above features will tend to favor the oxygen-bound species. Alternatively, the bent oxo-bridge (with increased pK_a) will tend to extract the

(53) Murray, K. S. *Coord. Chem. Rev.* **1973**, *12*, 1-37.
(54) Mukferjee, R. N.; Stack, T. D. P.; Holm, R. H. *J. Am. Chem. Soc.* **1988**, *110*, 1850.
(55) Ercolani, C.; Gardini, M.; Murray, K. S.; Pennesi, G.; Rossi, G. *Inorg. Chem.* **1986**, *25*, 3972.
(56) (a) Reem, R. C.; Solomon, E. I. *J. Am. Chem. Soc.* **1987**, *109*, 1216. (b) Reem, R. C.; Solomon, E. I. *J. Am. Chem. Soc.* **1984**, *106*, 8323.
(57) Atkin, C. L.; Thelander, L.; Reichard, P.; Lang, G. *J. Biol. Chem.* **1973**, *248*, 7464.
(58) (a) Schlosnagle, D. S.; Sander, E. G.; Bazer, F. W.; Roberts, R. M. *J. Biol. Chem.* **1976**, *251*, 4680. (b) Libscomb, J., private communication.
(59) One concern is that the similar intensities of the four absorbance bands implies comparable overlaps of both ligand orbitals with the iron d_{xy} and $d_{x^2-y^2}$ orbitals, which would indicate both orbitals have significant bonding character with the metal. However, this is not consistent with the Raman profile, as described above, and should be addressed through a calculation of the dimer electronic structure.
(60) Olivas, E.; deWaal, D. J. A.; Wilkins, R. G. *J. Inorg. Biochem.* **1979**, *11*, 205.
(61) Kurtz, D. M., Jr. Ph.D. Dissertation, Northwestern University, 1977.
(62) Taylor, R. C.; Cross, P. C. *J. Chem. Phys.* **1956**, *24*, 41.
(63) Dows, D. A.; Pimentel, G. C. *J. Chem. Phys.* **1955**, *23*, 1258.
(64) Rubinson, J. F.; Burgess, B. K.; Corbin, J. L.; Dilworth, M. J. *Biochemistry* **1985**, *24*, 273.
(65) Private communication with Professor Ronald E. Stenkamp, University of Washington.

proton, thus favoring reduction of the iron and causing the peroxide to be more reducing. This model will explain the rapid redox reactivity of deoxyHr with dioxygen relative to one-electron oxidants.[66] The latter produce rapid one-electron oxidation, but the second oxidation is slow, due either to the rearrangement necessary to make the oxo-bridged ferric site[67] or the poor electron transfer pathway through the hydroxo bridge. The oxidation upon oxygen binding is more rapid, since the bridge proton is removed to form the hydroperoxide, leaving the oxo-bridge. This structure should then be a better electron transfer pathway and be closer to the geometry of the met site, requiring a smaller structural rearrangement.

Acknowledgment. We thank NSF Grant DM8716199 for support of this research. R.L.M. acknowledges support from NIH AREA Grant 1R15GM36481 and thanks Jonathan Efron for his work in sample preparation. P.J.S. thanks the NIH for support of the NIR CD instrument at USC.

Registry No. Fe, 7439-89-6; O_2, 7782-44-7; $[(FeHEDTA)_2O]$, 47821-83-0.

Supplementary Material Available: Text and tables of dimer band energy additivities and optical electronegativities and various met and halfmetHr spectra (9 pages). Ordering information is given on any current masthead page.

(66) Bradic, Z.; Harrington, P. C.; Wilkins, R. G.; Yoneda, G. *Biochemistry* **1980**, *19*, 4149.

(67) (a) Armstrong, G. D.; Ramasan, T.; Sykes, A. G. *Inorg. Chem.* **1985**, *24*, 3230. (b) Armstrong, G. D.; Sykes, A. G. *Inorg. Chem.* **1987**, *26*, 3392. (c) Pearce, L. L.; Kurtz, D. M., Jr.; Xia, Y.; Debrunner, P. G. *J. Am. Chem. Soc.* **1987**, *109*, 7286.

Preresonance Raman Studies of Metal-to-Ligand Charge Transfer in $(NH_3)_4Ru(2,2'\text{-bpy})^{2+}$. In Situ Bond Length Changes, Force Constants, and Reorganization Energies

Stephen K. Doorn and Joseph T. Hupp*

Contribution from the Department of Chemistry, Northwestern University, Evanston, Illinois 60208. *Received June 30, 1988*

Abstract: As a prototype for charge-transfer reactions in general, the intense metal-to-ligand charge-transfer transition occurring in $Ru(NH_3)_4(bpy)^{2+}$ (bpy = 2,2'-bipyridine) has been examined experimentally by resonance and preresonance Raman spectroscopy and analytically by time-dependent scattering theory. To our knowledge, the present example represents the first application of the theory to charge-transfer problems. From the experiments and corresponding theory, the normal-coordinate changes accompanying the transition have been calculated. Both metal–ligand and intraligand bonds are found to distort significantly. When the distortion data are combined with the observed vibrational frequencies, a mode-by-mode assessment of the inner-shell reorganization energy is possible. Further experiments, in which the nature of the solvent is systematically varied, show that selected force constants (and therefore selected components of the internal reorganization energy) are modulated significantly (ca. 6–11%) by ligand–solvent hydrogen bonding. Finally, variations in the nature of the solvent are found to shift ground- and/or excited-state energies in such a way as to either enhance or attenuate the occurrence of net photochemistry.

Outer-sphere electron-transfer reactions, bridge-mediated inner-sphere reactions, and metal–ligand (ligand–metal) charge-transfer reactions constitute a near continuum of interrelated redox processes. Jortner has noted that the dark kinetics and relaxation dynamics of all three can be described in condensed phases by radiationless decay theory.[1] He[1] and others[2] further note that the familiar energy-gap law[3] and Marcus–Hush analysis[4,5] can be viewed as distinct limiting forms of the theory.[6] Regardless of the limiting form, however, nonradiative decay theory asserts that molecular structural changes will exert a profound influence upon the kinetics and dynamics of nearly all charge-transfer processes.

To elaborate, charge-transfer relaxation reactions can be broadly classified as either "weakly coupled" (i.e. highly exothermic, with inverted or nested potential energy surfaces) or "very strongly coupled" (i.e. thermoneutral or only moderately exothermic, with classically intersecting potential energy surfaces).[1,2] Further classification as either inter- or intramolecular (see above) is also possible. For all of these processes the structural changes of interest are the normal-coordinate distortions (Δ) or bond length changes (Δa), which accompany oxidation and reduction or charge redistribution. Collectively the effects of such changes have been handled theoretically in terms of inner-shell or bond reorganization energies (χ_i), where the calculation of χ_i also requires a knowledge of vibrational force constants (f).[4,5]

It should be further noted that any complete analysis of charge-transfer kinetics demands a knowledge of not only the total magnitude of χ_i but also the individual components. The reason for this is that weakly coupled processes make significant use of only high-frequency distortions (as vibrational acceptors for excited-state electronic energy) while strongly coupled processes directly entail only low-frequency distortions (as components of a classical activation barrier).

Obviously, in order to implement radiationless decay theory (or Marcus theory or related theories) as a tool for interpreting charge-transfer kinetics, it is necessary to have a detailed experimental knowledge of χ_i and its components. For very strongly coupled systems[7] the method of choice has been X-ray crystallography[8] (Δa) together with Raman scattering (f). On the other

(1) Jortner, J. *Philos. Mag.* **1979**, *40*, 317.

(2) See, for example: (2) Meyer, T. J. *Pure Appl. Chem.* **1986**, *58*, 1193. (b) Brunschwig, B. S.; Sutin, N. *Comments Inorg. Chem.* **1987**, *6*, 209.

(3) Representative papers: (a) Robinson, G. W.; Frosch, R. P. *J. Chem. Phys.* **1963**, *38*, 1187. (b) Siebrand, W.; Williams, D. F. *J. Chem. Phys.* **1967**, *46*, 403.

(4) Marcus, R. A. *J. Chem. Phys.* **1965**, *43*, 1261.

(5) Hush, N. S. *Prog. Inorg. Chem.* **1967**, *8*, 391.

(6) Energy-gap behavior can be simulated theoretically, for example, by setting all excited-state/ground-state vibrational overlaps (Franck-Condon factors) but one equal to zero. The nonzero overlap is the one involving the $v = 0$ level of the electronic excited state. On the other hand, approximate Marcus-type behavior can be obtained by allowing a nonzero overlap only at the vibrational energy level coinciding with the classical intersection point of the initial-state/final-state potential energy surfaces.

(7) Recent reviews: (a) Sutin, N. *Prog. Inorg. Chem.* **1983**, *30*, 441. (b) Sutin, N. *Acc. Chem. Res.* **1982**, *15*, 275. (c) Marcus, R. A.; Sutin, N. *Biochim. Biophys. Acta* **1985**, *811*, 265. (d) Cannon, R. D. *Electron Transfer Reactions*; Butterworths: London, 1980.

0002-7863/89/1511-4704$01.50/0